GPCR19 regulates P2X7R-mediated NLRP3 inflammasomal activation of microglia by Amyloid β in Alzheimer's diseases

Jahirul Islam
Seoul Natonal University https://orcid.org/0000-0003-3622-5255
Jung-Ah Cho
Wide River Institute of Immunology
Ju-yong Kim
Wide River Institute of Immunology
Kyung-Sun Park
Wide River Institute of Immunology
Young-Jae koh
Shaperon Inc. Ltd
Seung-Yong Seong (seongsy@snu.ac.kr)
Seoul Natonal University

Article

Keywords: Taurodeoxycholate, GPCR19, P2X7R, Alzheimer's disease, Neuroinflammation, Inflammasome

Posted Date: December 2nd, 2020

DOI: https://doi.org/10.21203/rs.3.rs-100024/v1

Abstract

Amyloid β (Aβ) and/or ATP activates NLRP3 inflammasome (N3I) by P2 × 7R ion channel of microglia, which is crucial in neuroinflammation shown in Alzheimer's disease (AD). Due to polymorphisms, subtypes, and ubiquitous expression of P2 × 7R, inhibition of P2 × 7R has not been effective for AD. We first report that GPCR19 is a prerequisite for P2 × 7R-mediated N3I activation and Taurodeoxycholate (TDCA), a GPCR19 ligand, inhibited the priming phase of N3I activation, suppressed P2 × 7R expression and P2 × 7R-mediated Ca^{++} mobilization, and N3I oligomerization which is essential for production of IL-1β/IL-18. Further, TDCA increased expression of scavenger receptor (SR) A, enhanced phagocytosis of Aβ, and decreased Aβ plaque numbers in the brain of 5x Familial Alzheimer's disease (5xFAD) mice. TDCA also reduced microgliosis, prevented neuronal loss, and improved memory function of 5xFAD mice. The pleiotropic roles of GPCR19 in P2 × 7-mediated N3I activation suggest that targeting GPCR19 might resolve neuroinflammation in AD patients.

Introduction

Despite Alzheimer's disease (AD) being the most common cause of dementia, no effective treatments are currently available[1]. Cholinergic, tau, and amyloid hypotheses have been suggested to explain the pathophysiology of AD[2]. Currently, the treatment of choices for AD patients are mostly based on cholinergic neurotransmission, which could not sufficiently mitigate the progression of AD[3]. Although the glial cells constitute brain cells more than neurons, neurons received more attention than glial cells for a long time, possibly due to prominent neurological symptoms of AD patients[4]. Within the last few years, however, clinical trials have moved to reduce neuroinflammation incurred by reactive microglia[5].

Neuroinflammation led by Aβ-activated microglia induces neuronal apoptosis in the hippocampus and cortex of AD patients[6]. In the brains of AD patients, pro-inflammatory mediators, such as reactive oxygen species (ROS), reactive nitrogen species (RNS), IL-1β, IL-6, and tumor necrosis factor (TNF)-α, are frequently increased[7]. The insoluble aggregates of Aβ and hyperphosphorylated tau, which make neurofibrillary tangles, are possibly main initiators of neuroinflammation in these patients[8]. These damage-associated molecular patterns (DAMPs) interact with pattern recognition receptors (PRR) on membranes of brain cells or in the cytosol to initiate pro-inflammatory pathways[9]. Sustained neuronal apoptosis may unleash more DAMPs in the brain, which further amplify sterile inflammation in the brain[10]. Considering that neuroinflammation plays crucial roles in the cognitive and memory deficits by neuronal loss, controlling neuroinflammation may provide promising therapeutic strategies[11].

The inflammasome plays central roles in the pathogenesis of many inflammatory disorders, including AD[12]. The NACHT, LRR, and PYD domains-containing protein 3 (NLRP3) polymorphisms are closely related with AD incidence[13]. Among the several inflammasomes, the most crucial contributor in AD pathologies is the NLRP3[14]. Aβ was efficiently cleared and cognition was improved in the AD mouse

model by inhibiting activation of the NLRP3 inflammasome (N3I)[15], suggesting that N3I is crucial in inflammatory neurodegeneration of AD[16].

The PRRs, such as CD36, CD14, TLR2, RAGE, and P2 × 7, of microglia are crucial in Aβ-triggered activation of the NLRP1 inflammasome (N1I) and N3I[17], which causes IL-1β/IL-18/pyroptosis-mediated inflammation in mice and in AD patients[13].

Unfortunately, however, strategies targeting components of N3I have not been successful in clinical trials for AD until now[18]. This may be due to redundant pro-inflammatory pathways activated by Aβ. For example, several PRRs recognize cytoplasmic tau and extracellular Aβ. Furthermore, the inflammasome is activated by canonical and non-canonical pathways, consisting of pro-caspase-1/4/5/11, gasdermin D, ASC, NLR proteins (such as NLRP1, NLRP3, NLRC4, NLRP6, or NLRP12), absent in melanoma 2 (AIM2), IFN-inducible protein 16 (IF116), and pyrin[19,20], although their roles in Aβ-mediated inflammasomal activation have not been elucidated in detail yet. The significance of redundancy in developing inflammasomal inhibitors was well demonstrated in studies using the NLRP3-specific inhibitor, MCC950[21]. MCC950 showed promising efficacy in preclinical settings, but not in clinical settings[22]. The redundancy of inflammasomal activation pathways implies evolutionary significance of the inflammasome responding to diverse environmental or endogenous threats to maintain tissue homeostasis[23]. For these reasons, a molecule at a higher level of the inflammasomal signaling cascade requires regulation to overcome redundancy in inflammasomal activation. A more plausible approach may involve targeting P2 × 7R, which is one of the top regulators of the signaling cascade necessary for N3I activation[24].

Brain cells, including microglia, express purinergic receptors, and both ionotropic P2X and metabotropic P2Y receptors are crucial in AD pathogenesis[25]. P2 × 7R is the ion-channel primarily studied in terms of N3I activation by Aβ[26]. Upon binding with ATP or Aβ, P2 × 7R renders cell membranes permeable to K^+ and Ca^{++}, which activate the inflammasome[27]. N3I of P2 × $7R^{-/-}$ microglia was not activated in response to Aβ[28], suggesting the essential role of P2 × 7R in Aβ-mediated neuroinflammation. P2 × 7R promotes the assembly of N3I, secretion of IL1β/18, and pyroptosis[29]. Intriguingly, the P2 × 7R is overexpressed in glial cells from AD patients and Aβ injection into the hippocampus increases P2 × 7R expression[30]. Taken together, the P2 × 7R plays a key role in chronic neuroinflammation and neurodegeneration in AD.

Apyrase blocks activation of N3I by Aβ[31], suggesting that ATP-P2 × 7R interaction is crucial in N3I activation in response to Aβ[32]. High levels of ATP are passively released from necrotic cells and act as a pro-inflammatory DAMP, binding to the P2 × 7R and activating the N3I[33]. P2 × 7R activation creates membrane pores, through which ATP can leak further[34].

Activation of P2 × 7R is also crucial in impairing phagocytosis of Aβ[35]. In AD patients, the phagocytic ability of microglia was insufficient to clear Aβ[5]. P2 × $7R^{-/-}$ microglia phagocytosed Aβ more efficiently

that wild type[36]. These findings clearly show both pro-inflammatory roles and anti-phagocytic functions of P2 × 7R in glial cells[37].

Thus, many P2 × 7R inhibitors have been developed to control inflammasomal activation without success until now[38]. These inhibitors effectively decreased inflammatory responses in AD mice[39]. However, many of these did not meet the clinical needs[40]. The human P2 × 7R is highly polymorphic and there are several isotypes[41]. Ten human P2 × 7R gene splice variants (P2 × 7RA–J) might produce a complex combination of P2 × 7R with various haplotypes that cause a broad spectrum of responsiveness to P2 × 7R inhibitors in clinical settings.

For these reasons, a non-polymorphic physiological regulator for P2 × 7R might be an alternative target to control inflammasome activation. We found that GPCR19 regulates P2 × 7R in N3I activation. TDCA, a GPCR19 agonist, inhibited the priming phase of N3I activation of microglia by activating adenylate cyclase, as reported earlier in other types of cells, and inhibited the activation phase of N3I by inhibiting P2 × 7R function.

Results

GPCR19 is a prerequisite for P2X7R-mediated Ca^{++} mobilization in microglia.

We sorted primary microglia using a magnetic column from the brains of C57BL/6 (B6), $P2X7^{-/-}$, and $GPCR19^{-/-}$ mice. The purity was above 95% (Supplementary Figure 1a). Upon treatment with ATP or BzATP, Ca^{++} mobilization significantly decreased in $P2X7R^{-/-}$ or in $GPCR19^{-/-}$ microglia compared with microglia from WT B6 (Figure 1a, 1b). GPCR19 and P2X7R were co-localized in primary microglia membranes (Figure 1c; Supplementary Figure 1b). ATP (Figure 1d) or BzATP (Figure 1e) increased Ca^{++} mobilization of BV2 microglia cells in the presence of Aβ, which was significantly inhibited by TDCA (400 ng/ml). When treated with Aβ and BzATP together, Ca^{++} mobilization of BV2 cells was significantly inhibited by TDCA in a dose-dependent manner (Figure 1f; Supplementary Figure 1c).

Treatment of BV2 cells with Aβ ± ATP significantly downregulated expression of GPCR19 on the cell surface, while this was recovered by TDCA treatment. On the contrary, the surface expression of P2X7R was upregulated by Aβ ± ATP, which was inhibited by TDCA treatment (Figure 1g, 1h; Supplementary Figure 2a). Although treatment with Aβ ± ATP also downregulated cytoplasmic GPCR19 expression in BV2 cells and upregulated cytoplasmic P2X7R expression, TDCA treatment for 1h did not normalize cytoplasmic expression levels of these two molecules (Supplementary Figure 2b~d). However, TDCA treatment for 24h significantly upregulated cytoplasmic GPCR19 expression which was suppressed by Aβ (Supplementary Figure 2e, 2f). GPCR19 expression in the frontal cortex of mice in the group of 5xFAD-TDCA (1 mg/kg, i.p., q.d. for 10 weeks) was significantly higher than that of mice in the group of 5xFAD-PBS (Figure 1i, 1k; Supplementary Figure 2g). The expression levels of P2X7R in the cortex of mice in the group of 5xFAD-TDCA (1 mg/kg, i.p., q.d. for 10 weeks) were significantly lower than that of mice in the group of 5xFAD-PBS (Figure 1j, 1k; Supplementary Figure 2h). The expression levels of GPCR19 in the

frontal cortex were significantly lower in six- or nine-month-old 5xFAD mice compared to that in three-month-old 5xFAD mice or B6 mice (Figure 1l, m). The expression levels of GPCR19 in the frontal cortex of six to nine-month-old 5xFAD mice did not differ significantly from that of three-month-old GPCR19$^{-/-}$ mice. Conversely, expression levels of P2X7R in the frontal cortex were significantly higher in three- to nine-month-old 5xFAD mice than in three-month-old B6 mice (Figure 1n, 1o). The expression level of P2X7R in the frontal cortex of nine-month-old 5xFAD mice was significantly higher than that of three-month-old 5xFAD mice.

TDCA suppresses N3I activation of microglia by Aβ ± ATP

When treated with Aβ ± ATP, transcript levels of NLRP3, ASC, Pro-Capase1, and ProIL-1β were increased in BV2 cells (Figure 2a). ATP alone could not increase these transcript levels except ProIL-1β. TDCA significantly inhibited upregulation of these transcripts by Aβ ± ATP.

In primary microglial cells, Aβ significantly increased expression of NLRP3 and ASC (Figure 2b, 2c). Treatment with Aβ + ATP further increased expression of NLRP3 and ASC. Without TDCA, NLRP3 colocalized with DAPI^{+} nucleus (white arrows), although the level of cytoplasmic NLRP3 also increased by treatment with Aβ ± ATP. TDCA treatment significantly suppressed expression of these two molecules, as well as their colocalization (yellow dots, Figure 2b, 2d; Supplementary Figure 3a). Interestingly, levels of nuclear NLRP3 (white arrows) were significantly downregulated by TDCA treatment. In the BV2 cell line, Aβ + ATP increased NLRP3 and ASC expression, but not by Aβ alone. As observed in primary microglia of mice, TDCA also suppressed expression and colocalization of NLRP3 and ASC in BV2 cells treated with Aβ + ATP (Supplementary Figure 3b~3e). Caspase-1 secretion from primary microglia (Figure 2e) or BV2 cells (Supplementary Figure 3f) treated with Aβ + ATP was inhibited by TDCA treatment.

To elucidate how TDCA inhibits transcription and expression of N3I components, we analyzed the GPCR19-cAMP-PKA-NF-kB axis after BV2 cells were treated with Aβ ± TDCA^{40}(Figure 2f~2l). TDCA increased cAMP production in BV2 cells irrespective of Aβ treatment (Figure 2f). Adenylyl cyclase inhibitor (KH7) blocked TDCA-mediated cAMP production in BV2 cells (Figure 2f). BV2 cells increased production of IL-1β, IL-18, and TNF-α upon treatment with Aβ ± ATP, while TDCA suppressed production of these cytokines (Figure 2g~2i). BV2 cells produced ROS in response to Aβ (Supplementary Figure 3g), and this was inhibited by TDCA treatment (Figure 2j).

In vivo, TDCA (1 mg/kg, i.p., q.d.) administration for 10 weeks decreased expression of NLRP3 and ASC in the frontal cortex of 5xFAD mice when compared with those of PBS-treated 5xFAD mice (Figure 2k, 2l; Supplementary Figure 3h).

Proteogenomic analysis of brain tissues of 5xFAD mice treated with TDCA

The proteomes of brain tissues from 5xFAD mice were analyzed post-administration of TDCA (1 mg/kg, i.p., q.d.) for 10 weeks (Figure 3a, 3b). In total, 3,259 unique proteins were identified at a protein threshold of a 1.0% false discovery rate. Among these proteins, 460 proteins showing peptide spectral counts in

more than two assays from triplicate assays, with a fold change of more than 2 between PBS- and TDCA-treated groups, are depicted on the heat map, plotted with the Perseus software platform (http://www.perseus-framework.org). Proteomic analysis indicated that 56 proteins exhibited more than 2-fold changes in the 95% confidence interval (Figure 3a), demonstrating two distinct proteome clusters that were upregulated in TDCA-treated groups and downregulated in PBS-treated groups, or vice versa. Functions of these proteins were further analyzed based on QIAGEN's IPA database (Figure 3b). Notably, a canonical pathway, 'Regulation of eIF4 and p70S6K', was enriched by TDCA treatment, suggesting that TDCA plays critical roles in translational regulation followed by calcium signaling, which could exert allosteric regulatory effects on many enzymes and proteins. Based on proteomic analysis, we further analyzed transcript levels of several pro-inflammatory cytokines in both the hippocampus and cortex of 5xFAD mice. The TDCA treatment for 10 weeks downregulated IL-1β, TNF-α, IL-33, 1L-12, CCL-11, and CCL-5 transcripts. On the contrary, increased transcripts of IFN-γ, IL-10, CCL-17, GPCR19, CD47, FPR-2, CD36, SRB1, and SRA in the brain of 5xFAD mice (Figure 3c).

TDCA increases expression of scavenger receptor (SR) A and phagocytosis of Aβ

We further investigated the effects of TDCA on SRA, since the expression of SRA was increased by TDCA treatment in the proteomic analysis of 5xFAD mice brains. *In vitro*, treatment of BV2 cells with Aβ significantly downregulated SRA expression and was normalized by TDCA (Figure 3d; Supplementary Figure 4a, 4b). SRA transcripts were significantly downregulated in BV2 cells upon treatment with Aβ for 24h and were dose-dependently increased by TDCA treatment (Supplementary Figure 4c). *In vivo*, $CD11b^{int}CD45^{int}$ primary microglia isolated from the brains of 5xFAD mice treated with TDCA for 10 weeks showed significantly higher SRA levels when compared with that of microglia from PBS-treated 5xFAD mice (Figure 3e). Since P2X7 is known to inhibit phagocytosis[35,37] and SRA is known to increase phagocytosis, we hypothesized that TDCA-induced suppression of P2X7 expression and TDCA-induced SRA expression might contribute to increased phagocytosis of Aβ by microglia. As expected, primary microglia from B6 mice showed decreased expression of P2X7R and increased phagocytosis of fluorescent Aβ oligomers (fAβ) upon treatment with TDCA (Figure 3f; Supplementary Figure 5a). Interestingly, $P2X7R^{high}$ microglia (white arrows) did not phagocytose fAβ even after treatment with TDCA (Figure 3f). After being phagocytosed, fAβ were co-localized with LAMP-2^{+} phagosomes in BV2 cells and the process was enhanced by TDCA treatment (Figure 3g; Supplementary Figure 5b).

TDCA decreases Aβ plaques and microgliosis in the brain of 5xFAD mice.

After i.p. administration of TDCA for 10 weeks, the numbers of Aβ plaques and the total area of plaques (white arrows) in the frontal cortex and in the hippocampus of 5xFAD mice were decreased (Figure 4a). Numbers of Iba-1^{+} reactive microglia in the frontal cortex (Figure 4b; Supplementary Figure 6a) and in the dentate gyrus (DG) of the hippocampus were decreased upon treatment with TDCA (Figure 4b, Supplementary Figure 6b). The number of $GFAP^{+}$ reactive astrocytes were also significantly decreased in the frontal cortex (Supplementary Figure 6c), DG (Supplementary Figure 6d), and CA3 regions (Supplementary Figure 6e) of the hippocampus in 5xFAD mice upon treatment with TDCA.

TDCA increases expression of immune-check point molecules on microglia

Based on proteomic analyses, we further investigated the expression of CD47, which is an immune checkpoint molecule in myeloid cells. CD47 expression was significantly downregulated by Aβ treatment in BV2 cells, and was inhibited by TDCA co-treatment (Figure 4c; Supplementary Figure 7a). Similarly, CD47 transcripts were downregulated by Aβ treatment in BV2 cells and were inhibited by TDCA co-treatment in a dose-dependent manner (Supplementary Figure 7b, 7c).

TDCA decreases the number of microglia and increases the number of MDSCs in the brains of 5xFAD mice

Brain cells were analyzed using FACS after 5xFAD mice received TDCA treatment for 10 weeks (1 mg/kg, i.p., q.d., Figure 5). $DAPI^-$ singlet cells were gated and expression of CD45 and CD11b were determined (Supplementary Figure 8a). The number of $CD45^{hi}CD11b^-$ lymphocytes (Supplementary Figure 8b), $CD45^{int}CD11b^{int}$ microglia (Figure 5c), $CD45^{int}CD11b^{hi}$ MDSCs (Figure 5d), and $CD45^{int}CD11b^{hi}Ly6C^{int}Ly6G^+$ PMN-MDSC (Figure 5e) were analyzed. $CD45^{hi}CD11b^-$ lymphocytes in 5xFAD mice were lower than that in age-matched B6 mice and were increased by TDCA treatment in 5xFAD mice (Supplementary Figure 8b). The number of $CD45^{int}CD11b^{int}$ microglia in 5xFAD mice treated with PBS was significantly higher than that in age-matched B6 mice (Figure 5c). After TDCA treatment for 10 weeks, the number of microglia was significantly lower than that observed in brains of 5xFAD mice treated with PBS (Figure 5c). Interestingly, the number of $CD45^{int}CD11b^{hi}$ MDSCs was significantly lower in PBS-treated 5xFAD mice than age-matched WT B6 mice and was higher in the TDCA-treated group when compared with the PBS-treated group of 5xFAD mice (Figure 5d). TDCA treatment did not change the number of $CD45^{hi}CD11b^+$ infiltrating cells (Supplementary Figure 8c) nor the number $CD11b^{hi}Ly6C^{hi}Ly6G^-$ M-MDSC (Supplementary Figure 8d). The number of $CD45^{int}CD11b^{hi}Ly6C^{int}Ly6G^+$ PMN-MDSCs in 5xFAD mice treated with PBS was lower than that in age-matched B6 mice (Figure 5e). However, the number of $CD45^{int}CD11b^{hi}Ly6C^{int}Ly6G^+$ PMN-MDSCs in 5xFAD mice treated with TDCA was significantly higher than that of 5xFAD mice treated with PBS (Figure 5e). To further test the effects of TDCA on trans-differentiation of microglia between M1/M2 phenotypes, primary microglia isolated from 1~2 days old B6 mice were treated with Aβ ± TDCA for 48 h in the presence of M-CSF (Supplementary Figure 8e). Treatment with Aβ *in vitro* decreased the number of $CD86^+CD206^+$ cells, while treatment with Aβ + TDCA increased the number of these cells (Figure 5f, 5g).

TDCA increases the number of PMN-MDSCs in the spleen of 5xFAD mice

5xFAD mice received TDCA (1 mg/kg, i.p., q.d.) for 10 weeks and the splenocytes were stained for FACS analysis. $DAPI^-CD45^+$ singlet cells were gated and the $CD11b^+$ cells were analyzed (Figure 6a; Supplementary Figure 9). The number of $Ly6C^{int}Ly6G^+$ PMN-MDSCs in the spleen of 5xFAD mice was significantly increased by TDCA treatment (Figure 6b). The number of $Ly6G^-Ly6C^{hi}$ M-MDSCs in the

spleen of 5xFAD mice treated with TDCA was significantly lower than that of PBS-treated 5xFAD mice (Figure 6c).

TDCA decreases apoptosis of neurons in 5xFAD mice brain

The $NeuN^+$ cells in the brains of 5xFAD mice were stained after treatment with TDCA for 10 weeks (1 mg/kg, i.p., q.d.). The frontal cortex and hippocampus (CA1, CA3, and DG) were observed using confocal microscopy (Figure 7a). $NeuN^+$ cells in the frontal cortex were significantly higher in 5xFAD mice treated with TDCA when compared to 5xFAD mice treated with PBS (Figure 7b; Supplementary Figure 10a). The mean fluorescent intensity (MFI) of $NeuN^+$ area in the hippocampus of 5xFAD mice was significantly higher in the TDCA group than the PBS group (Figure 7c, 7d; Supplementary Figure 10c ~ 10e).

Spatial learning and memory of 5xFAD mice.

B6 and 5xFAD mice were injected with PBS or TDCA for 10 weeks (1 mg/kg, i.p., q.d.), and spatial learning and memory were assessed using the Morris water maze (MWM) test (Supplementary Figure 11a). There were no significant changes in body weight after 10 weeks of TDCA treatment (Supplementary Figure 11b). Escape latency decreased over the 4 d training period in all three groups. The mice in the TDCA group showed significant reduction in time latency to platform (Figure 8a) in training and probe test which is comparable to B6 mice, while the escape latency was significantly shorter in the TDCA group compared to the PBS group. In the probe test at 5 d, TDCA-treated 5xFAD mice showed increased numbers of crossing the platform (Figure 8b). TDCA-treated 5xFAD mice remained in the target quadrant for longer periods of time than in the opposite quadrant, when compared with PBS-treated 5xFAD mice (Figure 8c). TDCA-treated 5xFAD mice spent more time in the platform compared to the PBS group (Supplementary Figure 11c). The time in the target quadrant and platform was comparable to those of B6 mice. 5xFAD mice treated with PBS were relatively random and disorganized compared with B6 mice and TDCA-treated 5xFAD mice (Figure 8d). The mean speed and total travel distance of 5xFAD mice was lower compared to B6 mice (Supplementary Figure 11d, 11e).

Spatial learning and memory were also assessed by the Y-maze test (Figure 8e) and Novel object recognition test (NOR) (Figure 8f, 8g). The % alternation of the mice in the 5xFAD-PBS group was significantly lower than that of mice in the B6-PBS group and 5xFAD-TDCA group (Figure 8e). However, the total number of arm entry did not differ significantly between the groups of mice (Supplementary Figure 11f). In the NOR test, exploration time to a new object compared to an old object was significantly higher in B6-PBS and 5xFAD-TDCA mice (Figure 8f). 5xFAD-PBS mice did not exhibit a difference in exploration time between old and new objects (Figure 8f). The discrimination index of the mice in the 5xFAD-TDCA group was significantly higher than that of mice in the 5xFAD-PBS group (Figure 8g).

After oral administration of TDCA (5 or 10 mg/kg, p.o., q.d.) for 14 weeks, spatial learning and memory of mice were also tested (Supplementary Figure 12a). No obvious changes in body weight were observed (Supplementary Figure 12b). Escape latency of mice in the 5xFAD-TDCA (10 mg/kg, p.o., q.d.) group decreased (Figure 8h), as much as observed in mice treated with TDCA i.p.. In the probe test at 5 d,

5xFAD-TDCA (10 mg/kg) mice exhibited increased numbers of crossings over the target quadrant (Figure 8i). 5xFAD-TDCA (10 mg/kg) mice remained in the target quadrant for longer periods of time and spent less time in the opposite quadrant when compared with 5xFAD-vehicle mice (Figure 8j). The mean speed and total travel distance of 5xFAD mice were similar between groups (Supplementary Figure 12c, 12d). Spatial learning and memory were also assessed by the Y-maze test after feeding TDCA orally (Figure 8k). The % alternation of the mice in the 5xFAD-vehicle group was significantly lower than that of mice in the 5xFAD-TDCA (10 mg/kg) group (Figure 8k).

Discussion

Senile Aβ plaques in the human brain incur microgliosis, which is responsible for neuroinflammatory cascades, causing memory and cognitive impairment, eventually progressing to dementia[6]. Reactive microgliosis accompanied by neuronal damages aggravates AD[5]. Aβ-mediated activation of N3I exacerbates the pathogenesis of AD by inducing neuroinflammaiton[14]. However, the intervention of N3I activation enough to suppress neuroinflammation of AD is still not successful. Therefore, many resources have been put forward to halt the progression of Aβ-mediated N3I activation, which might delay neuronal loss due to the neuroinflammatory cascade. In this study, we found that administration of a GPCR19 agonist, TDCA (1 mg/kg, i.p., q.d. or 10 mg/kg, p.o., q.d.), for 10 or 14 weeks, significantly improved learning and memory of 5xFAD mice (Fig. 8).

The possible mode of action of TDCA could be explained in four ways. First, TDCA could suppress the priming phase of N3I activation (transcription of NLRP3, ASC, and Pro-caspase-1) (Fig. 2a) and the activation phase of N3I (production of mature IL-1β and IL-18 by NLRP3-ASC oligomerization) (Fig. 2b-2 h) in response to Aβ and ATP. Second, TDCA could inhibit production of crucial proinflammatory mediators, such as ROS and TNF-α, of microglia independent of N3I activation (Fig. 2i, 2j). Third, TDCA could augment clearance of Aβ by enhancing phagocytosis and by suppressing P2 × 7 expression (Fig. 2f, 2j). Lastly, TDCA could increase the number of regulatory MDSCs in the brain that might further suppress neuroinflammation by Aβ (Fig. 5a, 5d). Overall, TDCA reduces neuroinflammation and prevents neuronal apoptosis, which delays impairment of spatial learning and memory (Fig. 7, 8).

TDCA regulates N3I activation by altering functions and expression of P2 × 7R after binding with GPCR19 (Fig. 1). The P2 × 7R on microglia is crucial in Ca^{++} mobilization that initiates N3I activation[42]. Many glial functions are mediated by Ca^{++}[30], such as production of cytokines and chemokines[43]. ATP released from damaged neurons could activate P2 × 7R in AD.

Upon stimulation with P2 × 7R agonists (ATP or BzATP), GPCR19$^{-/-}$ microglia could not mobilize cytosolic Ca^{++} as much as WT microglia (Fig. 1a, 1b), suggesting that GPCR19 is a prerequisite in Ca^{++} mobilization in response to P2 × 7R agonists within 100 sec. ATP enables the open state of the P2 × 7R on the cell membrane, thereby encouraging exchange of cytosolic and extracellular cations[44]. The crystal structure of the P2 × 7 receptor displays clear differences between the open and closed pore state[45].

However, none have been reported for the role of GPCR19 in this process until now. Several findings in this study suggest the bi-phasic role of GPCR19 in regulating P2 × 7R. In immediate phase in response to pro-inflammatory cues such as Aβ and/or ATP (50–150 sec), TDCA may regulate function of P2 × 7R by allosteric modulation of GPCR19 that interferes GPCR19-P2 × 7R interaction. GPCR19 and the P2 × 7R are co-localized on the cell membrane of resting microglia (Fig. 1) and Ca^{++} is mobilized within 100 sec in response to ATP. A GPCR19 agonist, TDCA, inhibited Ca^{++} mobilization when microglia were stimulated with Aβ + P2 × 7R agonist (ATP or BzATP) within 100 sec, further supporting the idea that GPCR19 is a prerequisite for the activation of P2 × 7R and TDCA interferes interaction of these two molecules (Fig. 1d-1f). The finding suggests that binding of TDCA with GPCR19 might cis-regulate opening the pore of the P2 × 7R. It is supposed that binding of TDCA with GPCR19 might alter tertiary structure of GPCR19 necessary for opening the pore of the P2 × 7R in response to its ligands. In delayed phase in response to Aβ and/or ATP (1 h), TDCA suppresses P2 × 7R expression and increases expression of GPCR19 on the cell membrane (Fig. 1g, 1 h), suggesting plausible trans-regulation of P2 × 7R expression by the GPCR19-mediated signaling cascade. In summary, the TDCA-GPCR19 complex might transmit signals necessary for inhibiting P2 × 7R expression on the membrane within an hour (delayed response) and might alter structures of GPCR19 necessary for Ca^{++} current incurred by P2 × 7R activation within a couple of seconds (immediate response) (Supplementary Fig. 13).

In the brains of nine-month-old 5xFAD mice, the expression of GPCR19 was significantly lower and the expression of P2 × 7R was significantly higher than levels observed in the brains of three-month-old 5xFAD mice or B6 mice (Fig. 1m, 1o). The expression levels of GPCR19 and P2 × 7R on microglia were reciprocally regulated after stimulation with Aβ ± ATP *in vitro*, which was reverted by TDCA treatment (Fig. 1g). Taken together, these findings suggest that neuroinflammation by Aβ might be responsible for downregulation of anti-inflammatory GPCR19 and upregulation of proinflammatory P2 × 7R upon aging. The relative expression levels of GPCR19 and P2 × 7R on microglia might be crucial biomarkers indicating the severity of neuroinflammation of AD patients.

P2 × 7R inhibits phagocytosis of Aβ in various pro-inflammatory microenvironments in AD[35]. TDCA enhanced phagocytosis of Aβ and coincided with downregulation of P2 × 7R expression in the microglia (Fig. 3f). Furthermore, TDCA treatment increased expression of SRA, which might further enhance phagocytosis of Aβ by microglia (Fig. 3g). Downregulation of P2 × 7R, which inhibits phagocytosis, and upregulation of SRA, which enhances phagocytosis, might explain the possible roles of TDCA in clearing Aβ plaques in the brain of 5xFAD mice *in vivo* (Fig. 4a).

Numbers of PMN-MDSCs significantly increased in the brain (Fig. 5e) and spleen (Fig. 6d) in the TDCA-treated group of mice. TDCA also increased the number of MDSCs in a mouse sepsis model[46]. In the sepsis model, the number of splenic $CD11b^{+}Gr1^{hi}CD244^{+}$ MDSCs significantly increased after i.v. infusion of TDCA (1 mg/kg)[46]. PMN-MDSC might suppress a broad spectrum of pro-inflammatory features in the AD brain, in addition to direct suppression of N3I pro-inflammatory pathways by TDCA. Proteomic analysis supports these ideas. Whole brain lysates exhibited global editing of the brain

proteome that leads to an anti-inflammatory microenvironment in the AD brain (Fig. 3a). For example, upregulation of clathrin-mediated endocytosis, FXR pathway, mTOR signaling, and acute phase response signaling, in addition to downregulation of NO signaling and PI3K/AKT signaling were observed after treatment with TDCA (Fig. 3b).

Various bile acids are GPCR19 agonists and could reduce inflammation in the brain[47]. However, many studies were carried out with bile acids in concentrations that are unobtainable in pharmacological or pathological conditions *in vivo*[48]. Thus, the exact role of bile acids in modulating brain inflammation in AD could not be concluded. In this study, we showed that TDCA, one of the bile acids interacting with GPCR19[49], could suppress brain inflammation in 5xFAD mice by inhibiting the P2 × 7R-N3I axis. Further, oral administration of TDCA also improved spatial learning and memory, as observed with i.p. injection of TDCA. Considering safety profiles of TDCA after i.v. administration[50], TDCA may provide a viable option for AD patients to ameliorate neuroinflammation that might delay progression of AD.

Materials And Methods

Reagents

TDCA was purchased from New Zealand Pharmaceuticals Ltd. (Palmerston North, New Zealand). KH7 (Ann Arbor, Michigan, USA) was dissolved in DMSO. ATP and BzATP (Sigma-Aldrich, St. Louis, MO, USA) were dissolved in PBS. 2% (v/v) Oleic acid (Croda, 4-3 Hitotsubashi 2-chome, Chiyoda-ku, Tokyo, Japan) and 4% (v/v) Monoolein (Gattefosse, Saint-priest, Cedex-France) were used to prepare the TDCA oral formulation.

Preparation of $A\beta_{1-42}$ oligomer

Lyophilized 0.1 mg vial of Amyloid β Protein Fragments$_{1-42}$ (Aβ) (Sigma-Aldrich) were dissolved into 50 µl DMSO (Sigma-Aldrich) for 1 h at room temperature with continuous rotation. Oligomeric $A\beta_{1-42}$ was prepared by diluting the dissolved Aβ into 100 µM concentration using DMEM/F12 media. The resulting solution was then incubated for 24 h at 4°C with continuous rotation.

Isolation of Primary Microglia and Culture

Primary microglia were obtained from cerebral cortices and hippocampi of male and female one~two-day-old B6 mice or adult B6, GPCR19$^{-/-}$, and P2X7R$^{-/-}$ mice (Jackson Laboratory, USA) using a mouse brain dissociation kit (Miltenyi Biotec GmbH, Bergisch, Gladbach, Germany). The tissue was cut into fragments using a scalpel blade (Medicom, Los Angeles, CA, USA) and then homogenized using gentleMACS$^{(TM)}$ C tube and gentleMACS^{TM} Octo Dissociator (Miltenyi Biotec GmbH). Single cell suspensions were obtained after passing the tissue homogenates through MACS^{R} Smart Strainers (70 µm) (Miltenyi Biotec GmbH). The myelin was depleted using a debris removal solution supplied with the kit. Microglia cells were isolated using CD11b MicroBeads, LS Columns, and a MACS multi stand system

(all obtained from Miltenyi Biotec GmbH). Isolated microglia were washed with PB buffer (0.5% FBS in PBS) and culture using DMEM-F12 media with 20% FBS and 10 ng/ml M-CSF (PeproTech, Rocky Hill, NJ) in a 95% air and 5% CO_2 atmosphere at 37°C for 48 h to stain cells with antibodies or for 24 h to stimulate cells.

For inflammasome activation, primary microglial cells from one~two-day-old B6 mice were seeded on 12 mm microscope cover glasses (Deckglaser, Luda-Konlgshofen, Germany) in 24 well PDL-coated cell culture plates (Corning, Wujiang, Jiangsu, China) at 7.5 x 10^4 cells/ml per well for 24 h, then serum starved for 10 h and treated with Aβ (2 μM), TDCA (400 ng/ml) for 24 h, and ATP (1 mM) for the final hour.

Cell culture

BV2 cell (Murin Microglial cell line) was maintained in a 95% air and 5% CO_2 atmosphere at 37°C in DMEM (Dulbecco's modified Eagle's medium complete media) (Invitrogen, Carlsbad, CA, USA) containing 10% FBS (Fetal Bovine Serum) (Invitrogen), and 1% penicillin and streptomycin (Invitrogen). BV2 cells were seeded in 6 well (1.5 x 10^5 cells/2 ml), 12 well (1 x 10^5 cells/ml), or 24 well (5 x 10^4 cells/0.5 ml) PDL-coated cell culture plates for 12 h using DMEM complete media. Cells were serum starved before treatment for 10 h using DMEM/F12 media (Thermo Fisher Scientific, Waltham, MA, USA). Cells were treated with Aβ (2 μM), TDCA (400 ng/ml), and ATP (1 mM) for 1 h in the case of GPCR-19, P2X7R interaction. For inflammasomal activation and inhibitor (KH7) assays, cells were treated with Aβ (2 μM), KH7 (4 μM), TDCA (400 ng/ml) for 24 h, and ATP (1 mM) for the final hour, DMEM/F12 media was used, unless stated otherwise. The cells were collected for RNA extraction and cell culture supernatant was used to analyze concentrations of cAMP, IL-1β, IL-18, TNF-α, and caspase-1 using ELISA.

Measurement of microglial Ca^{++} response

Adult mice microglial cells isolated from adult B6, GPCR19$^{-/-}$, and P2X7R$^{-/-}$ mice were seeded on 25 mm cover glasses (Deckglaser) in a 6 well plate. After 48 h culture with DMEM/F12 media containing 20% FBS and 10 ng/ml M-CSF in a 95% air and 5% CO_2 atmosphere at 37°C, cells with glass coverslips were transferred and loaded with 2 μM Fluo-4/AM for 30 min at 37°C in a physiological external solution consisting of 138 mM NaCl, 5.6 mM KCl, 0.5 mM MgCl2, 2 mM CaCl2, 10 mM HEPES, and 10 mM glucose (pH 7.4). After loading, cells on the coverslips were transferred to an open perfusion chamber and fluorescence was measured at 494/506 nm using a fluorescence microscope (Nikon, Tokyo, Japan). The microscope was equipped with an LED lamp (Andover, UK), integrated shutter, and cooled EM-CCD camera. The camera and shutter were controlled using MetaMorph software (Molecular Devices, Foster City, CA). Single cells were defined as regions of interest (ROIs). The 16-bit grayscale images with a binning of 1 x 1 were captured every 1 s with a ranging exposure time. Data were processed using OriginPro 8 software (OriginLab) and merged from three independent experiments.

BV2 cells were seeded on 25 mm cover glasses in a 6 well plate. After starvation, cells were treated with Aβ (2 μM) with or without TDCA (400 ng/ml) for 24 h. Cells with glass coverslips were transferred and loaded with 2 μM Fluo-4/AM for 30 min at 37°C in a physiological external solution mentioned above. After loading, cells were transferred to an open perfusion chamber and fluorescence was measured at 494/506 nm as previously described.

BV2 cell Ca^{++} sensing was measured using a BD calcium assay kit (BD bioscience, San Diego, CA, USA) according to the manufacturer's protocol. In a 6 well plate, 1.5 x 10^5 cells/2 ml media were treated with Aβ with or without TDCA for 24 h after serum starvation. Cells were harvested in a FACS tube from the cell culture plate, washed with complete RPMI media, loaded with loading dye, and incubated for 1 h at 37°C in a 5% CO_2 atmosphere. Cells were acquired for 1 min for basal signaling, then incubated with BzATP (300 μM) for 2 min, and recorded for an additional 4 min using flow cytometry (LSRFortessa, BD Biosciences, San Jose, CA, USA). Relative Fluorescent Units (RFU) were calculated using FlowJo version 9.0 (Treestar, Ashland, OR, USA).

Immunoblot

The cortex was harvested from B6, 5xFAD, GPCR19$^{-/-}$, and P2X7R$^{-/-}$ mice, lysed with RIPA buffer (Thermo Fisher Scientific, Meridian Road, Rockford, USA) supplemented with phosphatase inhibitor cocktail 2 (Sigma-Aldrich), and centrifuged to remove cell debris. The concentrations of the prepared protein samples were determined using a BCA kit (Thermo Fisher Scientific). Protein samples were separated by electrophoresis on 10% sodium dodecyl sulfate–polyacrylamide gels and then transferred electrophoretically to Immobilon, polyvinylidene difluoride membranes (Merck, Millipore, Billerica, MA, USA). The membranes were incubated at 4°C overnight with anti-GPCR19 polyclonal antibody (Novus Biologicals, Littleton, CO, USA), P2X7R monoclonal antibody (P2X7R (Clone 1F11, Biolegend, San Diego, CA, USA), and anti-β-actin (Sigma-Aldrich). The following day, the membranes were washed and then incubated with horseradish peroxidase-labeled anti-rabbit or anti-mouse secondary antibodies for 1 h at room temperature. Subsequently, membrane-bound horseradish peroxidase-labeled antibodies were detected using an enhanced chemiluminescence detection system, including the Pierce ECL Western Blotting Substrate (Thermo Fisher Scientific). Densitometric quantification of the bands was conducted using ImageJ software (Rasband, W.S, NIH, Maryland, USA). Protein levels were normalized to β-actin for quantification.

Immunocytochemistry

BV2 cells or primary microglia cells isolated from the adult mouse brain were seeded on 12 mm microscope cover glasses (Deckglaser) in 24 well plates. Cells were stained with anti-GPCR19 polyclonal antibody (Novus Biologicals) and P2X7R (Clone 1F11, Biolegend) with (cytoplasmic staining) or without permeabilization (surface staining) at 4°C overnight, followed by staining with goat anti-rabbit IgG, Alexa Fluor 488 (Thermo Fisher Scientific), and goat anti-rat IgG, Alexa Fluor 546 (Invitrogen) for 1 h at RT.

To stain inflammasomal components, BV2 or primary microglia cells isolated from the brains of one~two-day-old B6 mice were seeded on 12 mm microscope cover glasses in 24 well plates, and were treated with Aβ (2 μM), TDCA (400 ng/ml) for 24 h, and ATP (1 mM) for the final hour. The cells were permeabilized and stained with anti-NLRP3 polyclonal antibody (Abcam, Cambridge, United Kingdom) and anti-ASC antibody (Clone B-3, Santa Cruz Biotechnology, Inc. Dallas, Texas, USA) at 4°C overnight, followed by staining with secondary polyclonal antibodies, Alexa Flour 488-labeled goat anti-rabbit IgG, or Alexa Flour 532-labeled goat anti-mouse IgG (Invitrogen) for 1 h at RT.

To stain intracellular GPCR19 and cell surface CD47 and SRA, BV2 cells were treated with Aβ (2 μM) and TDCA (400 ng/ml) for 24 h. GPCR19 polyclonal antibody (Novus Biologicals), CD47 (GeneTex, Alton Pkwy Irvine, CA, USA), and CD204-SRA (Thermo Fisher Scientific) were used separately at 4°C overnight, followed by staining with goat anti-rabbit IgG, Alexa Fluor 488 (Thermo Fisher Scientific) for 1 h at RT.

For cytoplasmic staining, cells were treated with 0.3% Triton X-100 (Sigma-Aldrich, Steinheim, Germany) for 30 min. Control normal rabbit IgG (CST, Danvers, MA, USA), normal mouse IgG (Santa Cruz Biotechnology), or purified rat IgG (Biolegend) were used as experimental controls. After rinsing secondary polyclonal antibodies, cover glasses were placed on DAPI mounting solution (Vector laboratories, Burlingam, CA, USA) on glass slides. Fluorescence imaging was performed using Confocal Microscope A1 (Nikon, ECLIPSE Ti, New York, USA). The % co-localization of NLRP3-ASC was measured using ImageJ software after setting the color threshold caliper on the only yellow color. NIS-Elements.AR.lnk (version 4.2, Nikon) was used to measure mean fluorescence intensity (MFI) of ROI.

Quantitative RT-PCR

Cells were harvested after treatment and total RNA was isolated using a RNeasy Plus Mini kit (QIAGEN, Hilden, Germany). cDNA was prepared from 1 μg of total RNA using a Maxime RT PreMix kit (iNtRON Biotechnology, Gyeonggi-do, South Korea). Thereafter, real-time quantitative PCR (qPCR) was performed using SYBR Green Fast mix (Applied Biosystems, Woolston, Warrington, UK) and primers specific to target genes (Supplementary Table 1) in the StepOnePlus^{TM} Real-Time PCR system (Applied Biosystems, Marsiling Industrial Estate Road, Singapore). Expression levels of target mRNAs were analyzed using the ddCt method and were normalized to expression levels of mouse *GAPDH*, a housekeeping gene used as an endogenous control. All fold changes are expressed relative to the control group.

ELISA

Cell secreted cytokines were measured from cell culture supernatant using commercially available ELISA kits for Mouse IL-6, TNF-α, and IL-1β/IL-1F2 (R&D Systems, Minneapolis, MN, USA), IL-18 (MBL, Naka-Ku, Nagoya Aichi, Japan), and Caspase-1 (Novus Biologicals) according to the protocol supplied by the manufacturer. BV2 cells were cultured in the presence of Aβ (2 μM), TDCA (400 ng/ml), or KH7 (4 μM) for 24 h. Cells were harvested and lysed with 0.1 M HCl to measure intracellular cAMP using a cAMP Assay Kit (Abcam) according to the manufacturer's protocol.

Measurement of ROS production

BV2 cells were harvested in a FACS tube after treatment with Aβ (1~4 μM) and TDCA (400 ng/ml) for 24 h. Cells were washed with DPBS and incubated with 5 μM of 2'-7'-dichlorofluorescin diacetate (Invitrogen, Eugene, Oregon, US) in DMEM containing 1% penicillin and streptomycin for 30 min at room temperature in the dark. Samples were washed in DPBS, suspended in FACS buffer containing DAPI (0.3 μg/ml), then immediately acquired and analyzed using a BD LSR Fortessa flow cytometer (BD Bioscience, San Jose, CA, USA) and FlowJo v9 software.

Phagocytosis of Fluorescent Aβ oligomer

BV2 cells were seeded on microscope cover glasses in 24 well plates for confocal microscopy. Cells were treated with or without TDCA for 12 h. HilyteFluor™488 labeled Aβ (1-42) (AnaSpec, Freemont, CA, USA) were used for fluorescent Aβ oligomers as mentioned above. After pre-treatment with TDCA cells were incubated with fluorescent Aβ oligomers for 3 h, fixed with 4% paraformaldehyde (PFA), and permeabilized with 0.3% Triton X-100. After blocking, cells were incubated at 4°C overnight with primary antibody for LAMP2 (Clone M3/84, BD Pharmingen Inc, San Jose, CA, USA) or control rat IgG. After rinsing, cells were incubated with goat anti-Rat IgG (H+L) secondary Antibody (Invitrogen) for 1 h at room temperature in the dark. After rinsing, cover glasses were placed on the DAPI mounting solution on the glass slide. Fluorescence imaging was performed using Confocal Microscope A1. The % co-localization of fAβ-LAMP2 was measured using ImageJ software after setting the color threshold caliper on the only yellow color.

Primary microglia isolated from one~two-day-old B6 mice were cultured, pre-treated with TDCA (400 ng/ml) for 12 h and then incubated with fluorescent Aβ (1–42) oligomer (green) for 3 h. After incubation with f-Aβ, cells were washed with ice cold PBS and fixed with 4% paraformaldehyde (PFA). After blocking, cells were incubated at 4°C overnight with a primary antibody for P2X7R (Biolegend) or control IgG. Cells were then rinsed and incubated with Goat anti-Mouse IgG (H+L) Secondary Antibody (Invitrogen) for 1 h at room temperature in the dark. After rinsing, cover glasses were placed on the DAPI mounting solution on the glass slide. Fluorescence imaging was performed using Confocal Microscope A1. NIS-Elements.AR.lnk (version 4.2, Nikon) was used to measure mean fluorescence intensity (MFI) of ROI.

Animals

The 5xFAD mice co-overexpress high levels of APP with three FAD mutations (Swedish (K670N/M671L), Florida (I716V), and London (V717I)), and high levels of presenilins 1 (PSEN1) with two FAD mutations (M146L, L286V), which are specifically overexpressed in the brain, regulated by neural-specific Thy1 promoter[51]. 5xFAD mice were maintained by breeding male 5xFAD mice with female B6 mice. The SJL F1 hybrid was produced by an SJL male and a B6 female. PCR was performed for genotyping of the mice. 5xFAD or SJL mice were kindly provided by Professor Mook-Jung, In-hee or Professor Sung, Jung-Joon, respectively, of Seoul National University. All animal experiments were approved by the institutional animal care and use committees (IACUC) of Seoul National University (SNU-170517-25) and performed in

accordance with animal ethics regulations. Mice were maintained in specific pathogen-free conditions at the animal facility of Wide River Institute of Immunology.

Drug administration

5xFAD male and female mice (8 to 10 weeks old) were injected intraperitoneally (i.p.) with either 1 mg/kg of TDCA or PBS five times/week for ten weeks. Age and gender matched non-transgenic littermates were used as a control group. Behavioral tests were performed after treatment and then mice were sacrificed for further experimentation. In the case of oral (p.o.) treatment, 5 mg/kg or 10 mg/kg TDCA was mixed with Monoolein (1-Oleoyal-rac-glucerol) and Oleic acid (TDCA: Monoolein: Oleic acid = 1: 2: 1) in PBS. TDCA (5 or 10 mg/kg) or PBS p.o. were administered using gastric gavage five/week for 14 weeks. Behavioral tests were performed during the last two~three weeks of treatment.

Morris water maze test

The maze was composed of a circular pool (1.5 m in diameter, 80 cm in height) with spatial cues at three different locations. Before testing, the pool was filled with opaque water adjusted to 20 ± 1°C. On the first day, mice were allowed to freely swim in the water for 60 seconds to find the escape platform located in one quadrant of the pool. When they failed to find the platform, the mice were guided to the platform. Once on the platform, mice were allowed to remain there for 30 sec. From the next day for four consecutive days, the same procedure was repeated from three different starting points to train the mouse, and the time to reach the platform was recorded every day. After the four-day training period, the probe test was performed in the same manner, but without the platform. Each mouse was allowed to swim from one starting point for 60 seconds, which was recorded using a video camera. The video was analyzed for the movement of mice in the water using tracking software (SMART3.0, Panlab Harvard Apparatus, Barcelona, Spain) to count the number of crossings, the time on the platform, and to measure the time spent at each quadrant of the pool.

Y-maze test

Mouse functional behavior tests were performed on TDCA- or PBS-treated 5xFAD mice and WT (B6) control mice. The Y-maze test was assessed over the course of four days. On the first two days, individual mice were habituated to the task room and experimenter for 5 min. On the third day after task room and experimenter habituation, mice were allowed to habituate to the Y-maze for less than 1 min. On the last day, mice entered the middle of the Y-maze and were allowed to move freely within the maze for 8 min. Each mouse movement was recorded using a video camera. The video was analyzed for all mouse entries regarding limbs that pass through each half arm of the maze. Total arm entries and percentage of alteration were counted for each mouse and compared between groups of mice.

Novel object recognition test (NORT)

NORT was assessed over the course of four days. The apparatus consisted of a white acrylic box (350 mm x 450 mm x 250 mm). The basement of the box was divided into 6 equal rectangles. On the first two

days, each mouse was habituated to the box for 10 min. On the third day, two similar cylindrical objects were fixed in the box and mice were allowed to explore the objects freely for 10 min. On the last day, one cylindrical object was replaced by a similar size different object and the mouse explored this for 5 min. Exploration of two cylindrical objects on the third day, and exploration of the novel object and cylindrical object on day four was recorded for each mouse using a video camera. Total time and frequency of novel and old object exploration were counted for each mouse using the video footage. The percent discrimination index of the novel object was calculated from exploration time of novel and old object.

Flow cytometry analysis of brain and spleen cells

Cells from the isolated brain and spleen were prepared from TDCA- or PBS-administered mice after ten weeks of i.p. administration. In brief, mice were euthanized using Isoflurane (Hana Pharmaceutical, Korea) and cardiac perfused with ice-cold Dulbecco's PBS (Welgene; LB001-02). Brain cells were prepared using the Adult Brain Dissociation Kit, mouse and rat (Miltenyi Biotec GmbH) using the GentleMACS dissociator (Miltenyi Biotec GmbH) according to the manufacturer's protocol. A single cell suspension was obtained by passing the cell through a 70 μm cell strainer (MACS SmartStrainers, Miltenyi Biotec GmbH) and myelin was depleted using the percoll solution supplied with the Brain Dissociation Kit. Splenocytes were prepared by simply mincing and passing the whole spleen through a 40 μM nylon filter (BD Falcon, Bedford, MA). For lysis of red blood cells from splenocytes, cells were incubated with 2 ml of ammonium-chloride-potassium lysing buffer for 2 min. Cells were suspended in the FACS buffer: DPBS containing 1% FBS and 1 mM EDTA (Invitrogen). Cells were incubated with 2.5 ng purified anti-mouse CD16/32 mAb (Clone 2.4G2, BD Pharmingen) for 10^7 cells for 30 min on ice. Cells were stained with fluorochrome conjugated monoclonal antibodies: CD45-PerCP (Clone 30-F11), CD11b-APCcy7 (Clone: M1/70), Ly6C-FITC (Clone: AL21), and Ly6G-PE (Clone: 1A8, all obtained from BD Pharmingen) for 30 min at 4°C. Samples were washed in DPBS, suspended in a FACS buffer containing DAPI (0.3 μg/ml), and immediately acquired using flow cytometry (LSRFortessa, BD Biosciences). Further analysis was performed using FlowJo version 9.0. Total numbers of live brain cells and splenocytes were counted after Trypan blue staining, and cell subpopulations were calculated based on the % of total cells after FlowJo analysis.

Primary microglia isolated from one~two-day-old B6 mice were cultured and treated with Aβ (2 μM) and TDCA (400 ng/ml) for 48 h. Cells were harvested and incubated with CD86-PE-cy7 (Clone: GL1, BD Pharmingen) and CD206-PE (Clone: C068C2, Biolegend) for 30 min at 4°C. Samples were washed in DPBS, suspended in a FACS buffer containing DAPI (0.3 μg/ml), and immediately acquired using flow cytometry. Further analysis was performed using FlowJo.

Immunohistochemistry

TDCA- or PBS-treated 5xFAD or B6 mice were anesthetized and perfused with ice-cold PBS. Brains were harvested and maintained in 10% neutral buffer formalin (Sigma-Aldrich) for 24 h at 4°C and then embedded in paraffin (Lecia, Illinois, USA). The paraffin embedded brains were cut (3 μM) using

microtome (Thermo Fisher Scientific), then deparaffinized in xylene, and rehydrated in a graded ethanol series (100 %, 90%, 80%, and 70%). Antigen unmasking was performed by heating the brain sections in citrate-based buffer (pH 6, Vector laboratories, Burlingam, CA, USA). The sections were incubated in 0.3% Triton X-100 for 30 min at room temperature for intracellular staining, and then blocked with blocking solution of 10% normal goat serum (Thermo Fisher Scientific) and 1% BSA in PBS for 1 h. Tissue samples were incubated overnight at 4°C with the following primary antibodies: GPCR19 (Novus Biologicals), NLRP3 (Abcam), ASC (Santa Cruz Biotechnology), NeuN (Clone A60, Merk Millipore, Temecula, CA, USA), Iba-1 (Wako, Osaka, Japan), and GFAP (Thermo Fisher Scientific). Slices were subsequently incubated for 1 h at room temperature with Alexa 488, 532, or 546-conjugated IgG secondary antibodies, as appropriate, then counterstained with DAPI for 10 min

The Aβ core plaque was labeled by treating tissue with 1% Thioflavin-S (Sigma-Aldrich) in PBS for 10 min at room temperature after being deparaffinized in xylene and rehydrated in a graded ethanol series (100 %, 90%, 80%, and 70%). The tissue slides were then washed thrice with 70% ethanol following DW three times. Fluorescence imaging was performed using Confocal Microscope A1 (Nikon). NIS-Elements.AR.Ink (version 4.2, Nikon) was used to measure mean fluorescence intensity (MFI) of ROI.

Global protein profiling

Anesthetized Mice were perfused with cold PBS and the whole brain was extracted, followed by snap-freezing using liquid nitrogen. The frontal cortex and hippocampus region of each mouse was collected and digested using urea (8 M)-based in-solution digestion. After protein quantification using the BCA assay (Micro BCA Protein Assay Kit, Thermo Fisher Scientific, Bremen, Germany), samples were pooled together group by group and 300 µg of tissue extracts per group were separated via high pH reversed-phase fractionation using an Agilent 1260 HPLC infinity purification system (Agilent Technology, Santa Clara, CA, USA). The fractionated peptide samples were subsequently loaded onto traps (C18, 3 µm, 0.7 cm, Thermo Fisher Scientific) and EASY-Spray columns (C18, 2 µm, 100 Å, 50 cm, Thermo Fisher Scientific). Easy nano II Ultra Performance Liquid Chromatography and Q-Exactive Mass Spectrometry systems (Thermo Fisher Scientific) were used to separate the peptides. For Q-Exactive, a top 10 method was used. The Orbitrap mass analyzer was used to acquire full MS scans (m/z 300 - 1,600 range; resolution, 70,000). The Trans Proteomic Pipeline (Seattle Proteomic Center, Seattle, WA, USA) was used to convert the mass data files into mzXML files. Peptide masses were searched using a concatenated forward and reverse mouse international protein index (IPI) database (decoy ipi.MOUSE.v3.80 database, 54285 entries)[52] with the SEQUEST-Sorcerer platform (Thermo Fisher Scientific, Sage-N Research, Milpitas, CA). Sorcerer (Sage-N Research, Milpitas, CA, USA) was used to estimate the false discovery rate (FDR). Scaffold Q+ (Proteome Software, Portland, OR, USA) was used to compare spectral counts, validate MS/MS-based peptides, identify proteins (FDR < 1% in at least 2 peptides), and calculate Log2-fold changes (FC) and *P*-values (Student *t*-test). Differentially expressed proteins (FC >2, and *P* values <0.05) were uploaded to the web-based Ingenuity Pathway Analysis (IPA®) software (Version 26127183; QIAGEN) for functional analysis and protein interaction networks.

Statistical analysis

The data are expressed as the mean ± SEM and were analyzed using a two-sided, unpaired Student's *t* test. The mean value between groups were compared using GraphPad Prism 5.0 software (GraphPad Software, La Jolla, CA, USA), unless otherwise indicated. *P* values < 0.05 were considered statistically significant.

Declarations

Acknowledgments

This work was supported by a grant funded by the National Research Foundation, Ministry of Science, ICT and future planning (2012R1A5A2A44671346), a grant from the Korea Healthcare Technology R&D Project, Ministry of Health and Welfare (A062260), a grant from Gangwon Province, Republic of Korea, a grant from Chemon Co., Ltd (0654-20170002), a grant from Shaperon Inc. (0654-20200002) and a grant for Shaperon from Ministry of Health and Welfare (HI19C0429).

Author Contributions

JI performed all the experiments, helped data analysis and writing a manuscript unless otherwise specified. JA set up all preliminary experiments. JY helped with behavioral tests. KS helped with Ca^{++} studies. YJ helped in water maze. SYS conceived, supervised the project, analyzed DATA and wrote the manuscript.

Author information

Affiliations

Wide River Institute of Immunology, Seoul National University College of Medicine, Seoul Republic of Korea

Jahirul Islam, Jung-Ah Cho, Kyung-Sun Park, Ju-yong Kim and Seung-Yong Seong

Department of Biomedical Sciences, Seoul National University College of Medicine, Seoul Republic of Korea

Jahirul Islam and Seung-Yong Seong.

Department of Microbiology and Immunology, Seoul National University College of Medicine, Seoul Republic of Korea

Seung-Yong Seong.

Shaperon Inc. Ltd.

Young-Jae Koh, Seung-Yong Seong.

Competing interest

The patent “Pharmaceutical composition for prevention, treatment, or delay of Alzheimer's disease or dementia containing G protein-coupled receptor 19 agent as active ingredient: CN106794189, EP3248603, ES2750839, IN201747003504, JP2017523982, KR1020150095951, US20180104261” was invented by Seong *et.al*. and applied by Seoul National University R&DB Foundation. The exclusive license for the patent was transferred from SNU R&DB to Shaperon Inc. Dr S.Y. Seong is a founder of Shaperon Inc. and the current CEO.

References

1. Cunningham, E.L., McGuinness, B., Herron, B. & Passmore, A.P. Dementia. *Ulster Med J* **84**, 79–87 (2015).
2. Kametani, F. & Hasegawa, M. Reconsideration of Amyloid Hypothesis and Tau Hypothesis in Alzheimer's Disease. *Front Neurosci* **12**, 25 (2018).
3. Raschetti, R., Albanese, E., Vanacore, N. & Maggini, M. Cholinesterase inhibitors in mild cognitive impairment: a systematic review of randomised trials. *PLoS Med* **4**, e338 (2007).
4. Nirzhor, S.S.R., Khan, R.I. & Neelotpol, S. The Biology of Glial Cells and Their Complex Roles in Alzheimer's Disease: New Opportunities in Therapy. *Biomolecules* **8**(2018).
5. Hickman, S.E., Allison, E.K. & El Khoury, J. Microglial dysfunction and defective beta-amyloid clearance pathways in aging Alzheimer's disease mice. *The Journal of neuroscience: the official journal of the Society for Neuroscience* **28**, 8354–8360 (2008).
6. Hardy, J. & Higgins, G. Alzheimer's disease: the amyloid cascade hypothesis. *Science* **256**, 184–185 (1992).
7. Kinney, J.W., *et al.* Inflammation as a central mechanism in Alzheimer's disease. *Alzheimers Dement (N Y)* **4**, 575–590 (2018).
8. Kocahan, S. & Dogan, Z. Mechanisms of Alzheimer's Disease Pathogenesis and Prevention: The Brain, Neural Pathology, N-methyl-D-aspartate Receptors, Tau Protein and Other Risk Factors. *Clin Psychopharmacol Neurosci* **15**, 1–8 (2017).
9. Seong, S.Y. & Matzinger, P. Hydrophobicity: an ancient damage-associated molecular pattern that initiates innate immune responses. *Nat Rev Immunol* **4**, 469–478 (2004).
10. Zotova, E., Nicoll, J.A., Kalaria, R., Holmes, C. & Boche, D. Inflammation in Alzheimer's disease: relevance to pathogenesis and therapy. *Alzheimers Res Ther* **2**, 1 (2010).
11. Ardura-Fabregat, A., *et al.* Targeting Neuroinflammation to Treat Alzheimer's Disease. *CNS Drugs* **31**, 1057–1082 (2017).
12. Guo, H., Callaway, J.B. & Ting, J.P. Inflammasomes: mechanism of action, role in disease, and therapeutics. *Nat Med* **21**, 677–687 (2015).

13. Heneka, M.T., *et al.* NLRP3 is activated in Alzheimer's disease and contributes to pathology in APP/PS1 mice. *Nature* **493**, 674–678 (2013).
14. Tan, M.S., *et al.* NLRP3 polymorphisms are associated with late-onset Alzheimer's disease in Han Chinese. *J Neuroimmunol* **265**, 91–95 (2013).
15. Dempsey, C., *et al.* Inhibiting the NLRP3 inflammasome with MCC950 promotes non-phlogistic clearance of amyloid-β and cognitive function in APP/PS1 mice. *Brain Behav Immun* **61**, 306–316 (2017).
16. Tan, M.S., Yu, J.T., Jiang, T., Zhu, X.C. & Tan, L. The NLRP3 inflammasome in Alzheimer's disease. *Mol Neurobiol* **48**, 875–882 (2013).
17. Sheedy, F.J., *et al.* CD36 coordinates NLRP3 inflammasome activation by facilitating intracellular nucleation of soluble ligands into particulate ligands in sterile inflammation. *Nat Immunol* **14**, 812–820 (2013).
18. Mehta, D., Jackson, R., Paul, G., Shi, J. & Sabbagh, M. Why do trials for Alzheimer's disease drugs keep failing? A discontinued drug perspective for 2010–2015. *Expert Opin Investig Drugs* **26**, 735–739 (2017).
19. Broz, P. & Dixit, V.M. Inflammasomes: mechanism of assembly, regulation and signalling. *Nat Rev Immunol* **16**, 407–420 (2016).
20. Kerur, N., *et al.* IFI16 acts as a nuclear pathogen sensor to induce the inflammasome in response to Kaposi Sarcoma-associated herpesvirus infection. *Cell Host Microbe* **9**, 363–375 (2011).
21. Dong, Y., Li, X., Cheng, J. & Hou, L. Drug Development for Alzheimer's Disease: Microglia Induced Neuroinflammation as a Target? *Int J Mol Sci* **20**(2019).
22. Dempsey, C., *et al.* Inhibiting the NLRP3 inflammasome with MCC950 promotes non-phlogistic clearance of amyloid-beta and cognitive function in APP/PS1 mice. *Brain, behavior, and immunity* **61**, 306–316 (2017).
23. Rathinam, V.A.K. & Chan, F.K. Inflammasome, Inflammation, and Tissue Homeostasis. *Trends Mol Med* **24**, 304–318 (2018).
24. He, Y., Hara, H. & Núñez, G. Mechanism and Regulation of NLRP3 Inflammasome Activation. *Trends Biochem Sci* **41**, 1012–1021 (2016).
25. Burnstock, G. Purinergic Signalling and Neurological Diseases: An Update. *CNS Neurol Disord Drug Targets* **16**, 257–265 (2017).
26. Saez-Orellana, F., *et al.* P2X receptor overexpression induced by soluble oligomers of amyloid beta peptide potentiates synaptic failure and neuronal dyshomeostasis in cellular models of Alzheimer's disease. *Neuropharmacology* **128**, 366–378 (2018).
27. Abbracchio, M.P., Burnstock, G., Verkhratsky, A. & Zimmermann, H. Purinergic signalling in the nervous system: an overview. *Trends Neurosci* **32**, 19–29 (2009).
28. Sanz, J.M., *et al.* Activation of microglia by amyloid {beta} requires P2 × 7 receptor expression. *J Immunol* **182**, 4378–4385 (2009).

29. Karmakar, M., Katsnelson, M.A., Dubyak, G.R. & Pearlman, E. Neutrophil P2 × 7 receptors mediate NLRP3 inflammasome-dependent IL-1beta secretion in response to ATP. *Nat Commun* **7**, 10555 (2016).
30. McLarnon, J.G., Ryu, J.K., Walker, D.G. & Choi, H.B. Upregulated expression of purinergic P2 × (7) receptor in Alzheimer disease and amyloid-beta peptide-treated microglia and in peptide-injected rat hippocampus. *J Neuropathol Exp Neurol* **65**, 1090–1097 (2006).
31. Kelley, N., Jeltema, D., Duan, Y. & He, Y. The NLRP3 Inflammasome: An Overview of Mechanisms of Activation and Regulation. *Int J Mol Sci* **20**(2019).
32. Delekate, A., *et al.* Metabotropic P2Y1 receptor signalling mediates astrocytic hyperactivity in vivo in an Alzheimer's disease mouse model. *Nat Commun* **5**, 5422 (2014).
33. Gong, T., Liu, L., Jiang, W. & Zhou, R. DAMP-sensing receptors in sterile inflammation and inflammatory diseases. *Nat Rev Immunol* **20**, 95–112 (2020).
34. Kim, S.Y., Moon, J.H., Lee, H.G., Kim, S.U. & Lee, Y.B. ATP released from beta-amyloid-stimulated microglia induces reactive oxygen species production in an autocrine fashion. *Exp Mol Med* **39**, 820–827 (2007).
35. Gu, B.J. & Wiley, J.S. P2 × 7 as a scavenger receptor for innate phagocytosis in the brain. *Br J Pharmacol* **175**, 4195–4208 (2018).
36. Ni, J., Wang, P., Zhang, J., Chen, W. & Gu, L. Silencing of the P2 × (7) receptor enhances amyloid-beta phagocytosis by microglia. *Biochem Biophys Res Commun* **434**, 363–369 (2013).
37. Martin, E., *et al.* New role of P2 × 7 receptor in an Alzheimer's disease mouse model. *Mol Psychiatry* **24**, 108–125 (2019).
38. Albalawi, F., *et al.* The P2 × 7 Receptor Primes IL-1beta and the NLRP3 Inflammasome in Astrocytes Exposed to Mechanical Strain. *Front Cell Neurosci* **11**, 227 (2017).
39. Nizami, S., Hall-Roberts, H., Warrier, S., Cowley, S.A. & Di Daniel, E. Microglial inflammation and phagocytosis in Alzheimer's disease: Potential therapeutic targets. *Br J Pharmacol* **176**, 3515–3532 (2019).
40. Thawkar, B.S. & Kaur, G. Inhibitors of NF-κB and P2 × 7/NLRP3/Caspase 1 pathway in microglia: Novel therapeutic opportunities in neuroinflammation induced early-stage Alzheimer's disease. *J Neuroimmunol* **326**, 62–74 (2019).
41. Bartlett, R., Stokes, L. & Sluyter, R. The P2 × 7 receptor channel: recent developments and the use of P2 × 7 antagonists in models of disease. *Pharmacol Rev* **66**, 638–675 (2014).
42. Liu, Y.-H., *et al.* The ATP-P2 × 7 Signaling Axis Is an Essential Sentinel for Intracellular Clostridium difficile Pathogen-Induced Inflammasome Activation. *Frontiers in Cellular and Infection Microbiology* **8**(2018).
43. Hoffmann, A., Kann, O., Ohlemeyer, C., Hanisch, U.K. & Kettenmann, H. Elevation of basal intracellular calcium as a central element in the activation of brain macrophages (microglia): suppression of receptor-evoked calcium signaling and control of release function. *The Journal of neuroscience: the official journal of the Society for Neuroscience* **23**, 4410–4419 (2003).

44. Khakh, B.S. & North, R.A. Neuromodulation by extracellular ATP and P2X receptors in the CNS. *Neuron* **76**, 51–69 (2012).
45. Karasawa, A. & Kawate, T. Expression and Purification of a Mammalian P2 × 7 Receptor from Sf9 Insect Cells. *Bio Protoc* **7**(2017).
46. Chang, S., *et al.* Taurodeoxycholate Increases the Number of Myeloid-Derived Suppressor Cells That Ameliorate Sepsis in Mice. *Front Immunol* **9**, 1984 (2018).
47. McMillin, M., *et al.* TGR5 signaling reduces neuroinflammation during hepatic encephalopathy. *J Neurochem* **135**, 565–576 (2015).
48. Guo, C., *et al.* Bile Acids Control Inflammation and Metabolic Disorder through Inhibition of NLRP3 Inflammasome. *Immunity* **45**, 802–816 (2016).
49. Wan, Y.Y. & Sheng, L. Regulation of bile acid receptor activity(). *Liver Res* **2**, 180–185 (2018).
50. Choi, H.J., *et al.* Nonclinical toxicology studies with sodium taurodeoxycholate: acute and subacute toxicity in dogs. *Drug Chem Toxicol*, 1–9 (2019).
51. Oakley, H., *et al.* Intraneuronal beta-amyloid aggregates, neurodegeneration, and neuron loss in transgenic mice with five familial Alzheimer's disease mutations: potential factors in amyloid plaque formation. *The Journal of neuroscience: the official journal of the Society for Neuroscience* **26**, 10129–10140 (2006).
52. Kersey, P.J., *et al.* The International Protein Index: an integrated database for proteomics experiments. *Proteomics* **4**, 1985–1988 (2004).

Figures

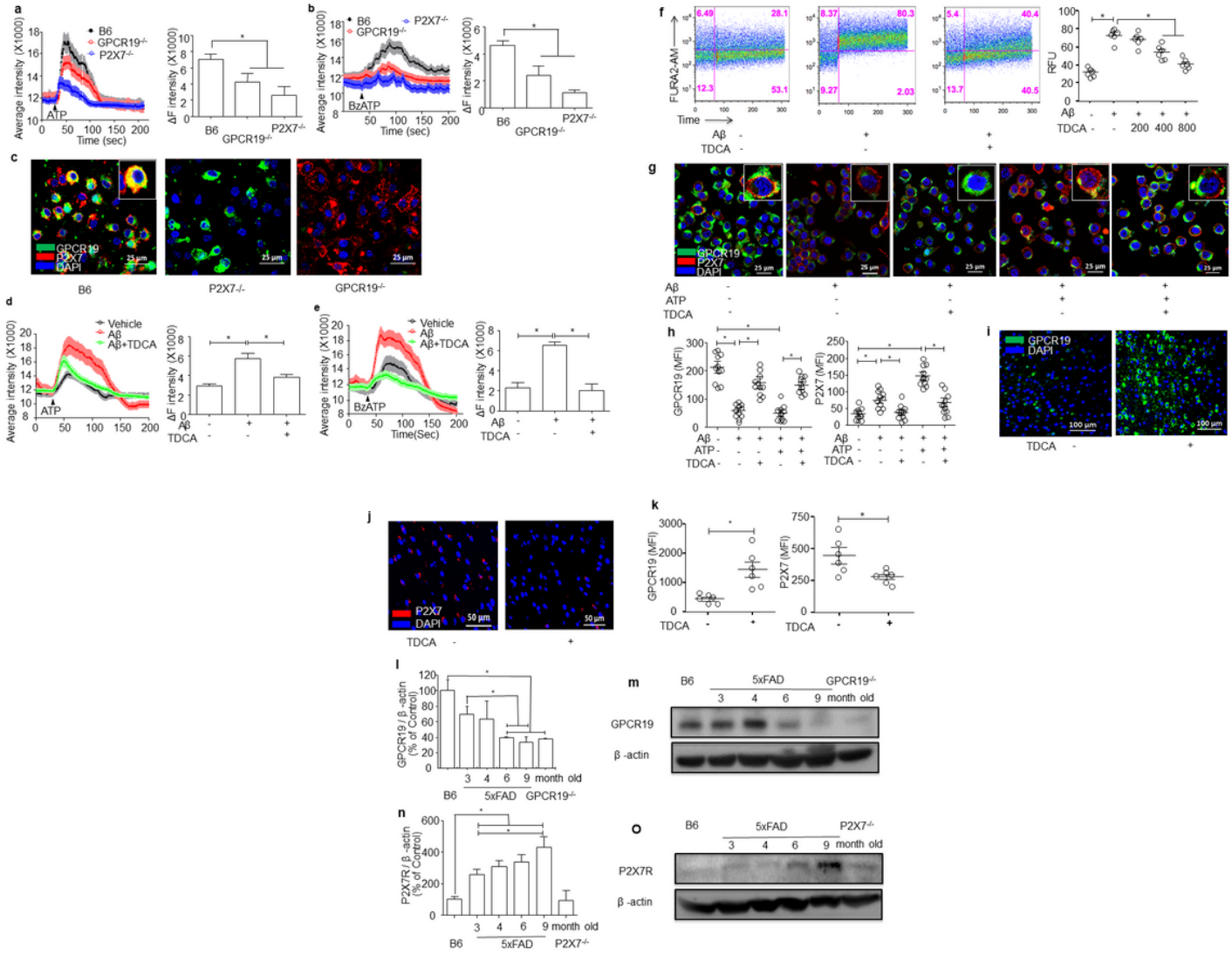

Figure 1

GPCR19 is a prerequisite for P2X7R-mediated Ca++ mobilization in microglia. a, b, The primary microglia from B6, GPCR19-/-, and P2X7R-/- mice (n = 6/group) were stimulated with ATP (a) or BzATP (b) (40 μM). Average intensity reflecting intracellular Ca++ mobilization (shown in left panels) and delta intensity (max-min) after stimulation was analyzed (right panel). c, Co-localization of GPCR19 and P2X7 on membranes of primary microglia are shown using confocal microscopy. d, e, The representative plots (left panels) of three independent experiments (right panels) showing Ca++ mobilization of BV2 cells in response to Aβ (2 μM) and TDCA (400 ng/ml) in presence of ATP (d) or BzATP (e) are depicted. f, Ca++ mobilization of BV2 cells treated with Aβ (2 μM) and TDCA (200~800 ng/ml) in response to BzATP (300 μM) was measured using flow-cytometry. The representative FACS plots (left panels) of three independent experiments (right panels) are depicted. g, The expression levels of GPCR19 (green) and P2X7R (Red) on the surface of BV2 cells were analyzed using confocal microscopy after treatment with Aβ (2 μM), ATP (1 mM), and/or TDCA (400 ng/ml) for 1 h. h, MFI ± SEM of 4~5 ROI (× 600) from panel g were analyzed. Expression levels of GPCR19 (i) and P2X7R (j) in the frontal cortex of 5xFAD mice (n = 6/group) were analyzed using confocal microscopy after treatment with 1 mg/kg TDCA i.p for ten weeks.

k, MFI ± SEM of 2~3 ROI (× 200) from panel i and j were analyzed. m, GPCR19 expression and o, P2X7R expression levels in the frontal cortex of B6, 5xFAD, GPCR19-/-, and P2X7R-/- mice were analyzed using WB. The expression levels of GPCR19 (l) and P2X7R (n) in B6 mice were considered as 100%. The individual samples are shown with the mean ± SEM. *P < 0.05 using the Student's unpaired t-test.

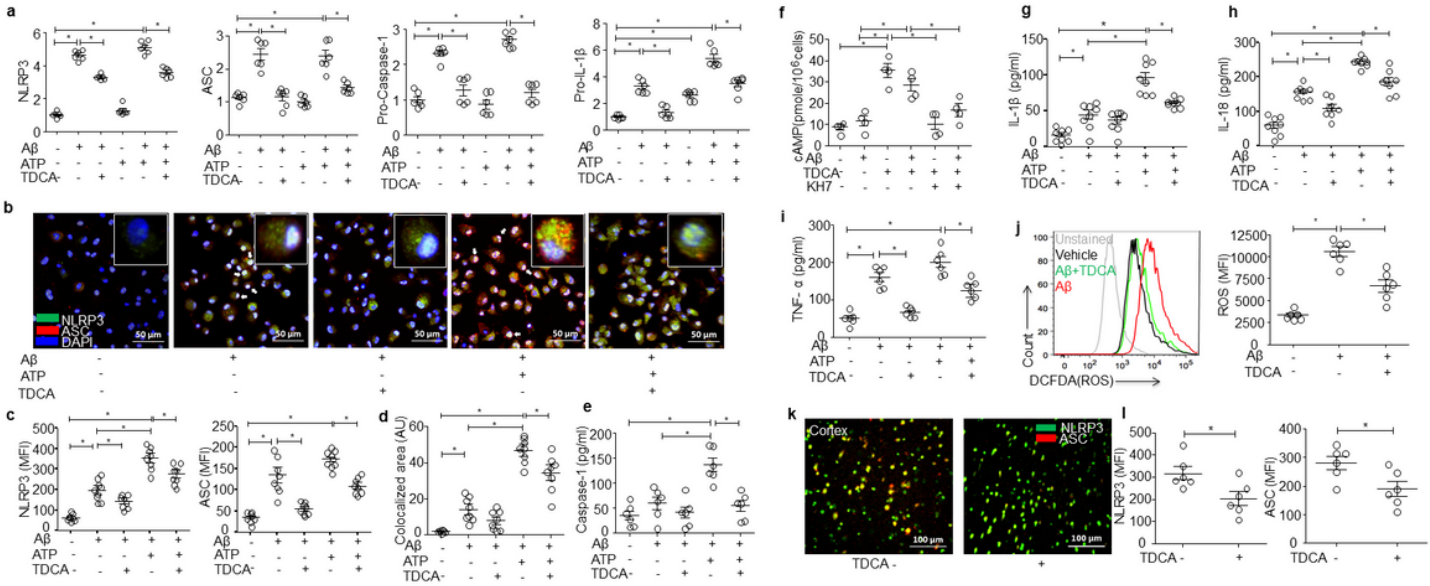

Figure 2

TDCA suppress activation of NLRP3-Inflammasome of microglia. a, mRNA expression of inflammasomal components: NLRP3, ASC, Pro-Caspase-1, and IL-1β were tested using qPCR in BV2 cells. Cells were treated with Aβ (2 μM) and TDCA (400 ng/ml) for 24 h and ATP (1 mM) for the last 1 h. Gene expressions were normalized using GAPDH. b, Representative Immuno-fluorescent microscopic images of primary microglia cells that were co-immuno-stained for NLRP3 (green) and ASC (red) followed by DAPI mounting for nucleus (blue). Primary microglia from B6 were treated with Aβ (2 μM) and TDCA (400 ng/ml) for 24 h and ATP (1 mM) for the last 1 h. c, MFI ± SEM of 4~5 ROI (× 600) from panel b were analyzed. d, Inflammasomal complexes from merged images of NLRP3 and ASC (yellow) as colocalized areas were analyzed using Image J. e, Concentrations of caspase-1 in culture supernatants of primary microglial cells were analyzed using ELISA. Concentrations of cAMP (f), IL-1β (g), IL-18 (h), and TNF-α (i) in culture supernatants of BV2 cells were analyzed using ELISA. Cells were incubated with Aβ (2 μM), TDCA (400 ng/ml), KH7 (4 μM) for 24 h, and ATP (1 mM) for the last 1 h. j, ROS production in BV2 cells was quantitated using FACS after pulsing cells with DCFDA. A representative FACS plot (left panel) of three independent experiments (right panel) is depicted. k, Confocal microscopy showing cytoplasmic NLRP-3 (green) and ASC (red) expression in the cortex of 5xFAD mice (n = 6/group) treated with 1 mg/kg TDCA i.p for ten weeks. l, MFI ± SEM of 2~3 ROI (× 200) from panel k was analyzed. The individual samples are shown with the mean ± SEM. *P < 0.05 using the Student's unpaired t-test.

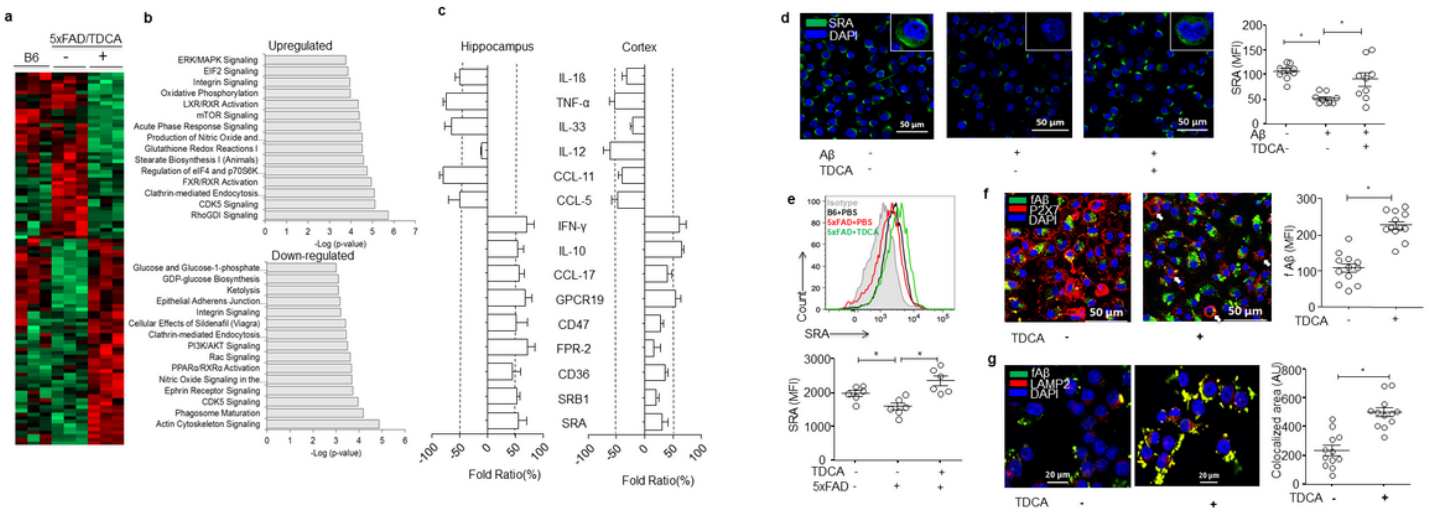

Figure 3

Proteomic analyses of mice brain and enhanced phagocytosis of Aβ by TDCA. B6 (5xFAD-) or 5xFAD (n = 6/group) mice were treated with 1 mg/kg TDCA/PBS i.p for ten weeks. a, The heat map shows proteomic profiling of brain lysates expressed differentially (FC > 2 and FDR q< 0.1) between groups. Each row represents a single protein and each column represents an individual sample. b, The top 15 canonical pathways consisting of proteins “upregulated” or “downregulated” by treatment with TDCA are shown. c, The cytokines, chemokines, immune-checkpoint molecules, and scavenger receptors expressed in the hippocampus and cortex were determined by qPCR. Fold ratio denotes the ratio between CtTDCA and Ctvehicle, where a ratio less than zero indicates that the expression was inhibited upon TDCA treatment. d, BV2 microglia cells were treated with Aβ (2 μM) and TDCA (400 ng/ml) to determine surface expression of SRA (green) using confocal Microscopy. MFI ± SEM of 4~5 ROI (× 600) from the left panel of three independent experiments were analyzed in the right panel. e, Surface expression of SRA on CD11bintCD45int microglial cells from 5xFAD or B6 mice was determined using flow cytometry. A representative FACS plot (upper panel) and MFI ± SEM of n = 6 mice/group (lower panel) were analyzed. f, TDCA (400 ng/ml) effects on phagocytosis of fluorescent Aβ by primary microglia isolated from B6 were determined using confocal microscopy. g, TDCA (400 ng/ml) effects on phagocytosis of fluorescent Aβ and co-localization with phagosome marker LAMP2 on BV2 cells were determined using confocal microscopy. MFI ± SEM of 4~5 ROI (× 600) from the left panel of f and g were analyzed. The individual samples are shown with the mean ± SEM. *P < 0.05 using the Student's unpaired t-test.

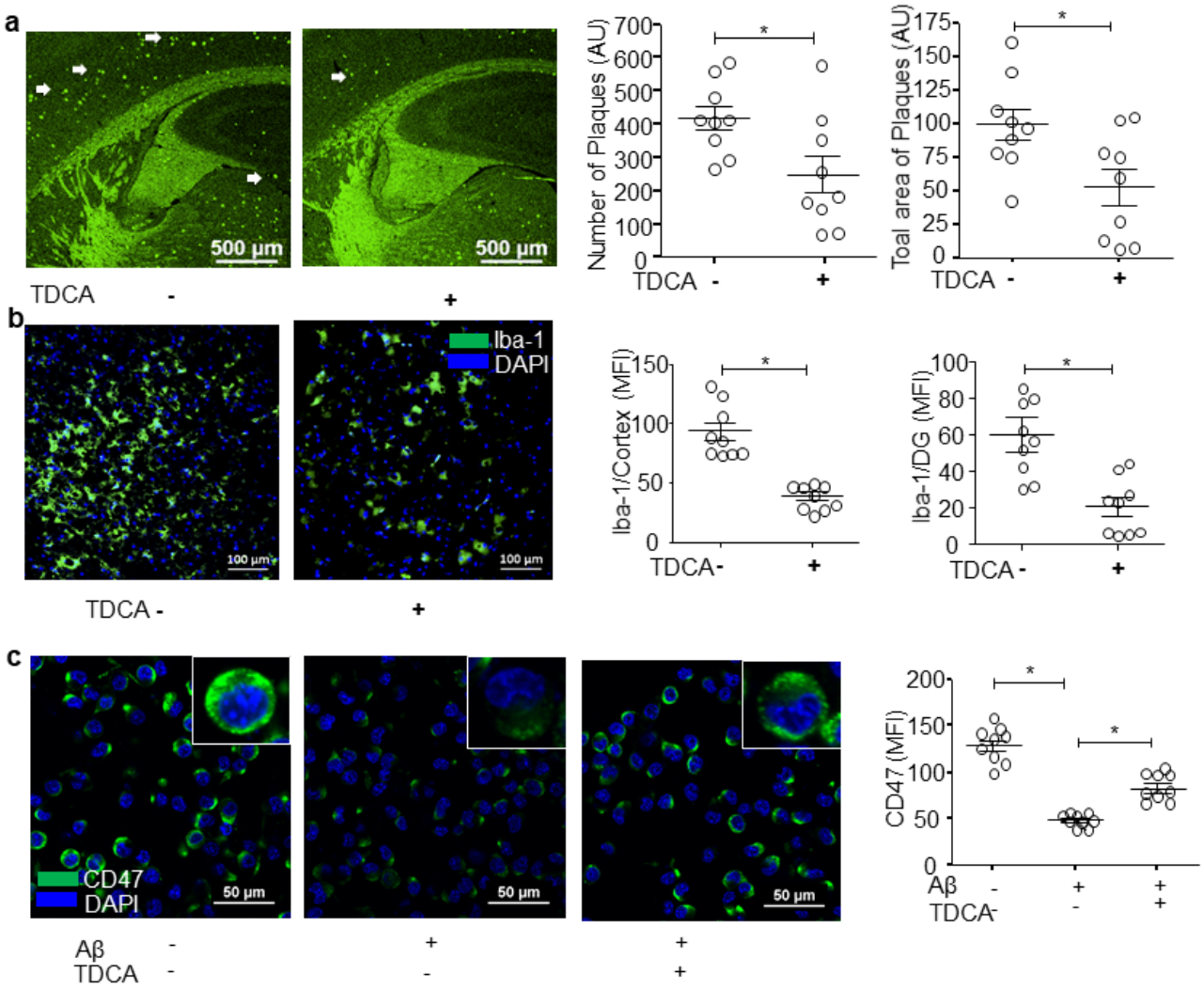

Figure 4

The number of Aβ plaques and microglia in 5xFAD mouse brain The 5xFAD mice (n = 9/group) were treated with TDCA (1 mg/kg, i.p) for ten weeks. a, Paraffin sections of brains were stained with Thioflavin-S to show Aβ plaques (green dots indicated with white arrows) in the left panel. The number of plaques and total area of plaques were quantitated using Image J after selecting a random field from each brain sample at 100 × magnification. b, Frozen sections of 5xFAD mice brain were stained with Iba-1 showing reactive microglia in the left panel. MFI ± SEM of a specific ROI (× 200) from the cortex (panel b) and DG region were analyzed in right panels. c, Confocal microscopy showing cell surface expression of CD47 (green) on BV2 microglia treated with Aβ (2 μM) and TDCA (400 ng/ml) in the left panel. MFI ± SEM of 4~5 ROI (× 600) from the left panel of three independent experiments were analyzed (right panel). The individual samples are shown with the mean ± SEM. *P < 0.05 using the Student's unpaired t-test.

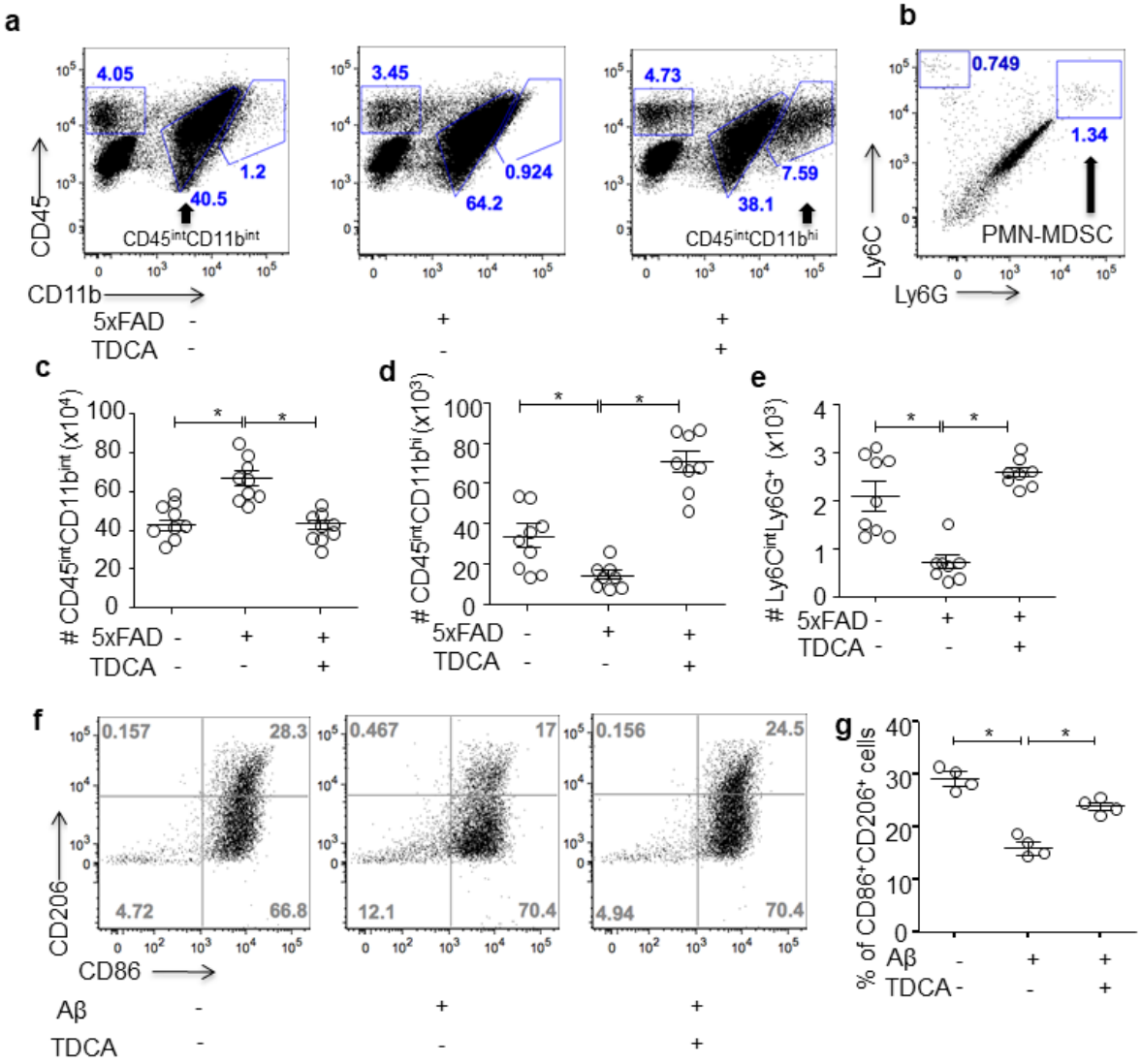

Figure 5

TDCA increases PMN-MDSCs in 5xFAD mouse brain and M2 phenotype of microglia. a, The representative FACS plots are depicted from the DAPI- viable cells. B6 (5xFAD-) and 5xFAD mice were treated with 1 mg/kg TDCA i.p., q.d. for ten weeks (n= 8~9/group). CD45intCD11bint microglia, CD45hiCD11bint Infiltrating cells, CD45hiCD11b− lymphocytes and CD45intCD11bhi MDSCs were analyzed. b, CD45intCD11bhicells were gated for the expression of Ly6C and Ly6G. c, The number of CD45intCD11bint microglial cells d, CD45intCD11bhi MDSCs and e, CD45intCD11bhiLy6G+ PMN-MDSC were analyzed and compared between groups of mice. f, Primary microglia cultured in the presence of 10 ng/ml M-CSF were treated with Aβ (2 μM) and TDCA (400 ng/ml) for 48 h and immune-stained for CD86 and CD206 expression. g, % of CD86+CD206+ cells were compared between groups. The individual samples (open circles) are shown with the mean ± SEM. *, P < 0.05 using the Student's unpaired t-test.

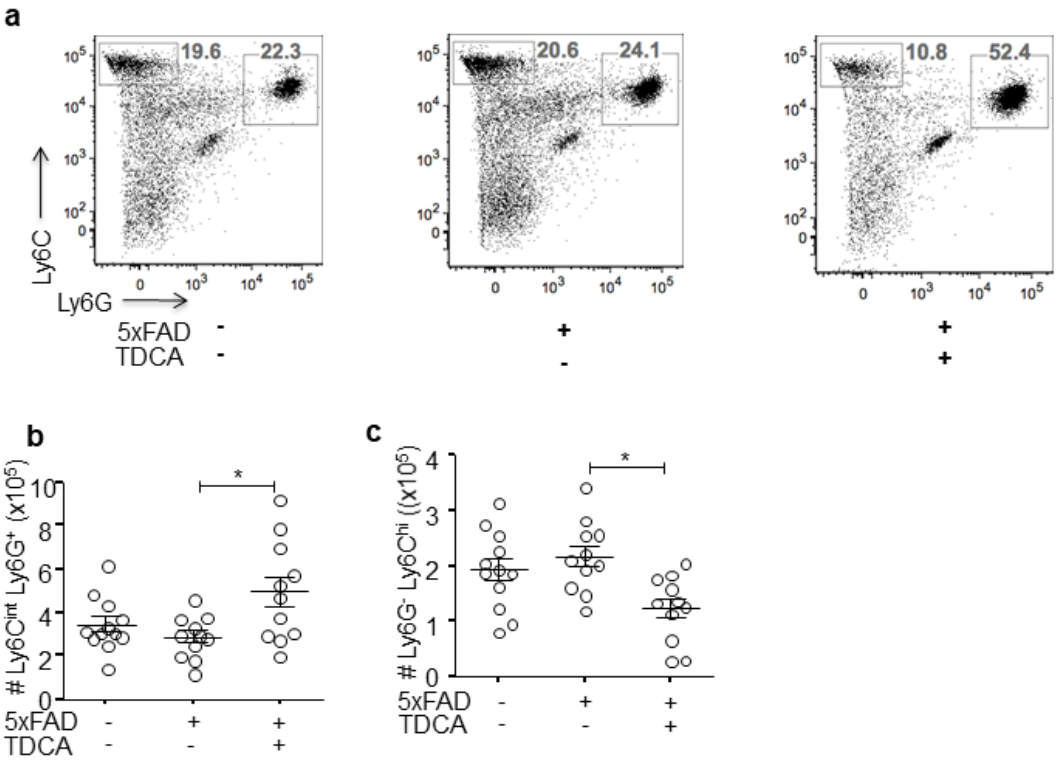

Figure 6

TDCA increases number of PMN-MDSCs in 5xFAD mouse spleen. Changes in number of myeloid cells in the spleen of B6 (5xFAD-) and 5xFAD mice (n = 10~12/group) after treatment with 1 mg/kg TDCA i.p., q.d. for ten weeks. a, DAPI negative, CD45+CD11b+ cells were analyzed for the expression of Ly6C and Ly6G, and representative FACS plots are shown. b, The number of CD11b+Ly6CintLy6G+cells and c, the number of CD11b+Ly6ChiLy6G- cells were counted and compared. The individual samples are shown with the mean ± SEM. *P < 0.05 using the Student's unpaired t-test.

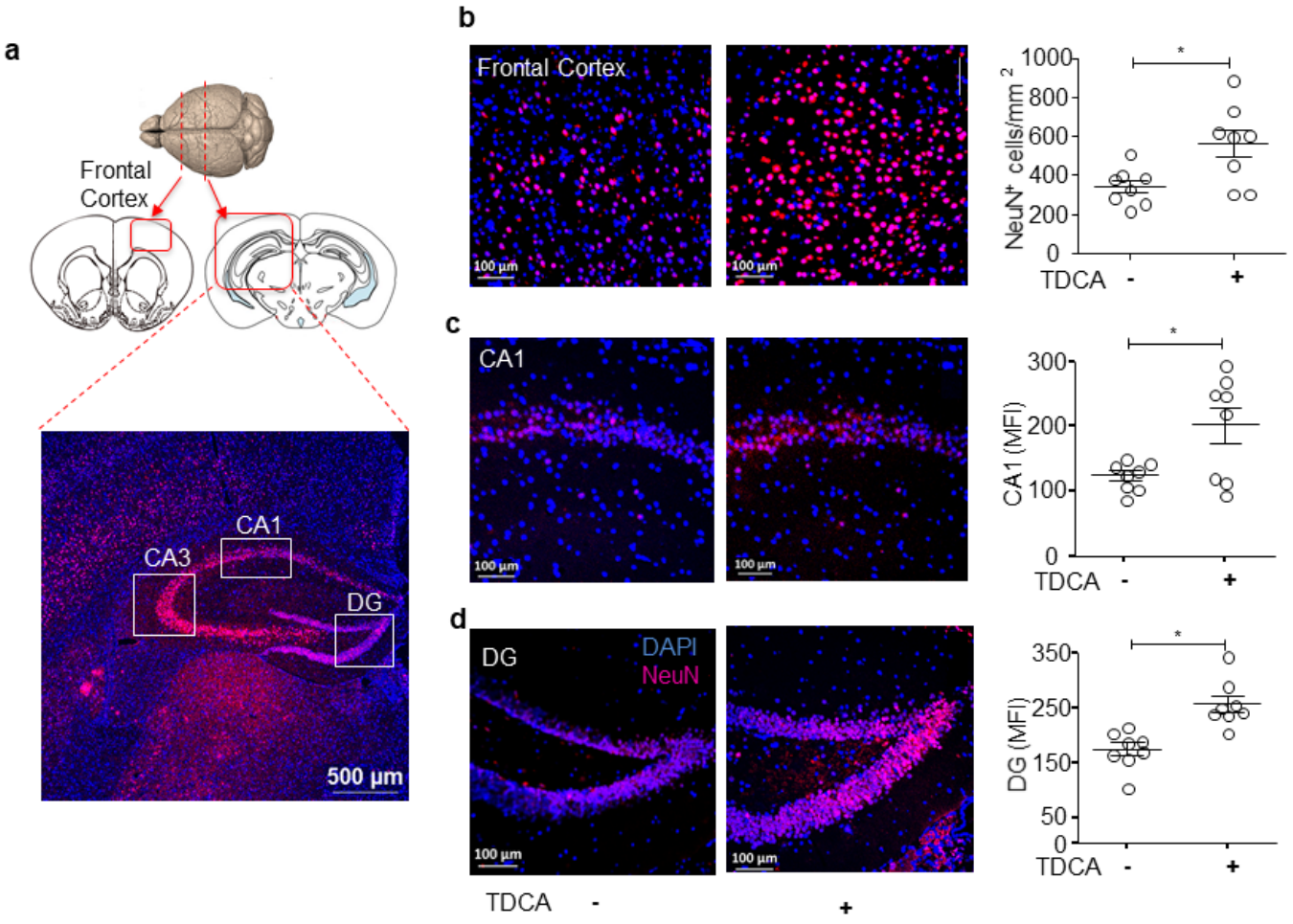

Figure 7

TDCA prevents neuronal apoptosis in 5xFAD mouse brain. Confocal microscopy showing NeuN+ cells in frontal cortex, CA, and DG of 5xFAD mice (n = 8/group) treated with 1 mg/kg TDCA i.p., q.d. for ten weeks. a, The paraffin sections were made from regions indicated as frontal cortex, CA, and DG. b, The number of NeuN+ cells were enumerated after staining sections of the frontal cortex. The MFI of ROIs of sections was quantitated from the section of c, CA1 and d, DG at 200 × magnification. A set of the representative images are depicted in the left panel and the pooled data of number of NeuN+ cells or MFI ± SEM are shown in the right panel. The nuclei were stained with DAPI (blue). The individual samples are shown with the mean ± SEM. *P < 0.05 using the Student's unpaired t-test.

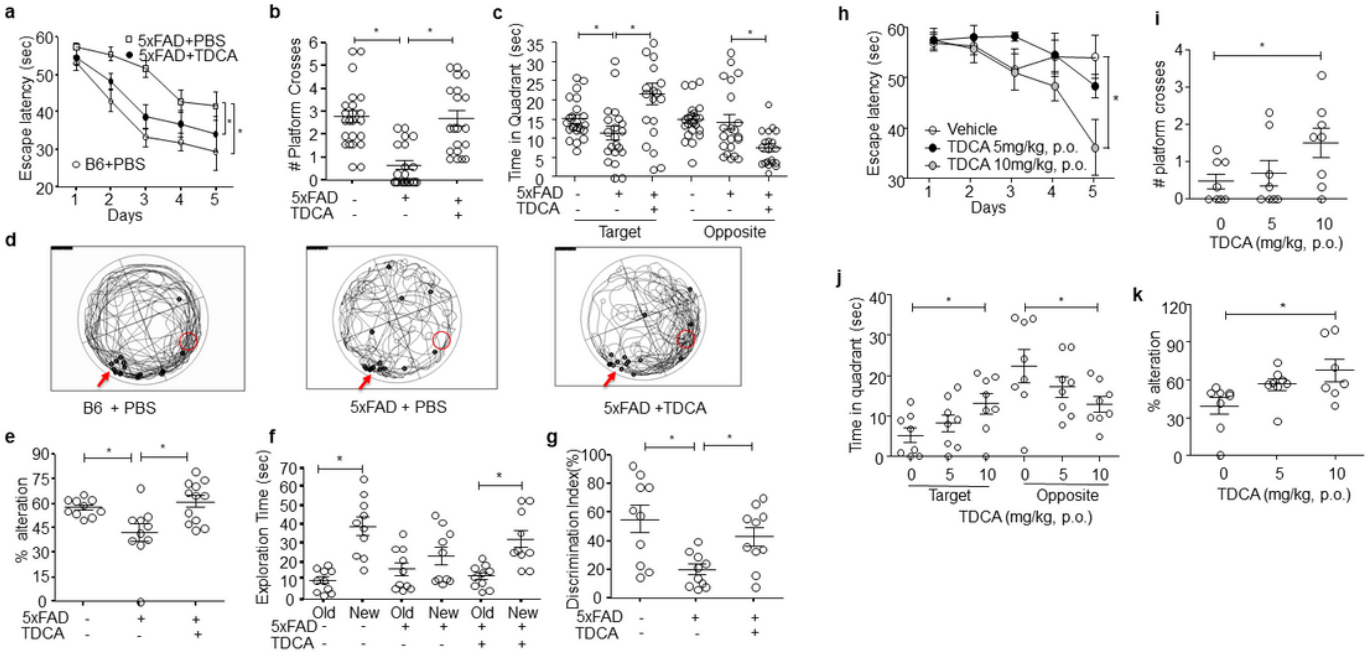

Figure 8

TDCA improves spatial learning and memory of 5xFAD mouse. Memory of 5xFAD and B6 (5xFAD-) mice was tested after treatment with 1 mg/kg TDCA i.p., q.d. for ten weeks in three separate experiments (n = 20~22/group). a, Escape latency: time to reach the hidden platform, b, Number of platform crosses, and c, time in target (platform located) and opposite quadrant were measured by using the MWM test. d, The trajectory maps showing the escape route of mice in the MWM test in one set of experiments for all mice. The red arrows and red circles indicate release points and positions of the platform, respectively. Black dots indicate the end points for individual mice. e, Alteration percentages of mice (n = 9~12) in the Y maze test were calculated by; 100 × # spontaneous alteration / # of total arm entry. f, Total exploration time for each object of individual mice in the NOR test are depicted. g, Discrimination index (%) = 100 × time spent to explore novel object / exploration time for both novel and old object for each mouse (n = 10). Memory of 5xFAD and B6 mice (n = 8/group) were tested using the MWM test and the Y maze test after feeding the mice with TDCA (5 or 10 mg/kg) for 14 weeks (h ~ k). h, Escape latency l, Number of platform crosses and j, time in target and opposite quadrant were measured using the MWM test. k, Alteration percentages in the Y maze test were calculated. The individual samples are shown with the mean ± SEM. *P < 0.05 using the Student's unpaired t-test.

Supplementary Files

This is a list of supplementary files associated with this preprint. Click to download.

- AlzMainSFigures201029.pptx
- AlzMainSFigures201029.pptx
- AlzMainSFigures201029.pptx